Time Interleaved RF Carrier Modulations and Demodulations

Kwang-Jin Koh, *Member, IEEE*, Seyed Yahya Mortazavi, *Student Member, IEEE*, and Sadia Afroz, *Student Member, IEEE*

***Abstract*—This paper proposes a time-interleaved RF carrier modulation and demodulation technique, suitable for high frequency mixer applications under a constraint of active device speed limitation. The presents are in essence mixer arrays where modulated outputs by a series of time-delayed carriers with a reduced frequency, compared with a carrier frequency in fundamental mixers, will be interleaved in the time domain to synthesize the final output. The mixer arrays inherit an FIR filtering function, and the time interleaving process is equivalent to the filtering process where the arrays select the fundamental tone or its harmonics of a carrier in a periodic manner. The carrier waveform and duty-cycle play important roles in the noise performance of the mixer arrays. A comprehensive noise analysis is presented in this paper for both cases of correlated-noise and uncorrelated-noise mixer arrays. To minimize output noise power, optimization of carrier duty-cycle and noise filtering technique have been proposed and analyzed extensively for various types of carrier pulse. Finally analytical mismatch models are provided and output SNR degradations under finite mismatches amongst mixer array elements have been discussed based on the mismatch models. All theoretical analyses are verified through behavioral mixer array simulations including Monte-Carlo statistical simulations.**

***Index Terms*—Array, demodulator, FIR filter, mixer, mixer array, modulator, multiphase, radio frequency, time interleaving, transversal filter, wireless communications.**

I. Introduction

RECENTLY wireless communications at millimeter (mm)-wave and submillimeter wave ranges have been gaining growing attentions to achieve a high data-rate over several 10's Gb/s [1]–[3]. One of key technical huddles in realizing the high-speed communications in integrated circuit technologies is the carrier modulations and demodulations, due to a lack of carrier source having a high spectral purity with an adequate output power at such high frequencies. To circumvent the issue from the system perspective, heterodyne architectures have been adopted to reduce required carrier frequency at the expense of a hardware complexity and image issue involved in the double conversions [4]–[6]. A subharmonic mixing (e.g., 2x, 4x even-harmonic carrier modulation) has been another popular choice for a minimum amount of signal processing at the mm-waves and therefore to relieve the speed burden on the local oscillator (LO) paths in the mm-wave mixer designs [7]–[9]. A constant progress has also been made to push oscillation frequency of voltage controlled oscillators over sub-terahertz realms in solid-state electronics [10]–[12]. Yet because of a limited active device speed, major challenges have been posed in implementing practical carrier modulation and demodulation systems with a fundamental mixer at the high-end of the mm-wave regimes [12].

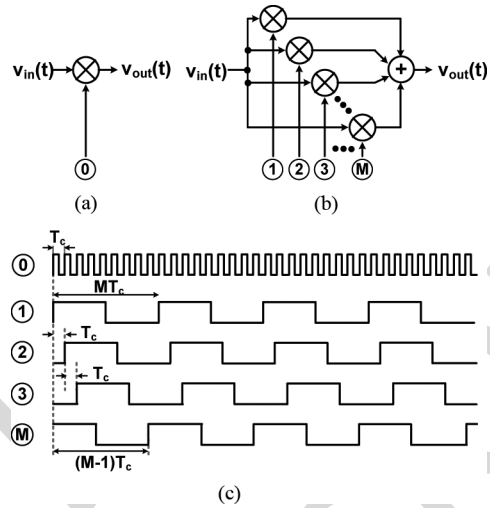

Fig. 1. (a) Fundamental mixer (modulation frequency: $f_c = 1/T_c$), (b) time-interleaved (TI) mixer array with a time-interleaving factor of M (modulation frequency: f_c/M), and (c) rectangular pulse trains for the fundamental mixer and the TI mixer arrays.

In this paper, a time-interleaved carrier modulation and demodulation technique has been proposed to enable mm-wave and submillimeter wave frequency mixers under the constraints of the device speed limitations. Fig. 1(b) illustrates a time-interleaved carrier modulator which is essentially a mixer array where each mixer modulates the input signal with a reduced frequency, compared with the fundamental mixer in Fig. 1(a). By interleaving the modulated outputs from individual mixers, the final output will contain the same frequency information as in the fundamental mixer. An essential benefit in the time-interleaved modulation is that the carrier frequency can be reduced by a factor of the number of time interleaving. This allows less speed burden on electronics generating carrier signals, which will be a particular benefit when realizing high-speed communication electronics in silicon processes suffering from a relatively low device speed compared with that of compound semiconductors [13]–[15].

The time-interleaved mixer arrays inherit a filtering function of a transversal filter [16], and the interleaving process is essentially a filtering process where fundamental tone and its harmonics of a carrier can be filtered selectively, which is elaborated in Section II. The waveform and duty-cycle of carriers

Manuscript received February 12, 2013; revised May 17, 2013; accepted June 24, 2013. This paper was recommended by Associate Editor J. Ma.

The authors are with the Department of Electrical and Computer Engineering, Virginia Tech, Blacksburg, VA 24061 USA (e-mail: kkoh@vt.edu).

Color versions of one or more of the figures in this paper are available online at http://ieeexplore.ieee.org.

Digital Object Identifier 10.1109/TCSI.2013.2278387

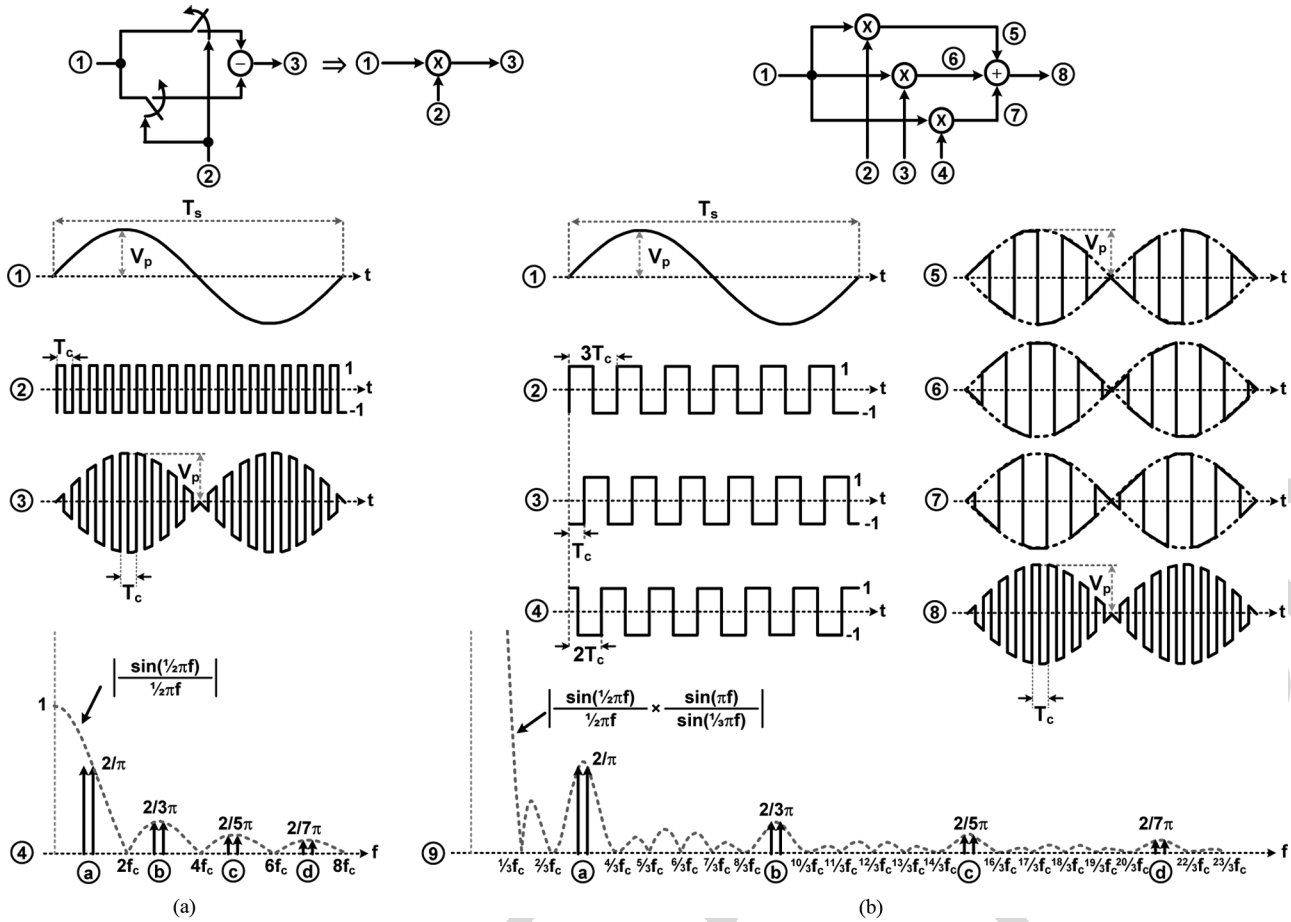

Fig. 2. Fundamental and time-interleaved carrier modulations with bipolar differential carriers: (a) modulation with fundamental carrier frequency using bipolar *on-off* switches (①:input signal; ②: bipolar rectangular carrier pulse; ③: modulated output; and ④: spectral components of the output normalized by the input peak magnitude), (b) time-interleaved modulation with $1/3f_c$ of carrier frequency (time interleaving factor: 3, ①: input signal; ②, ③ and ④: bipolar rectangular *subcarrier* pulses; ⑤, ⑥ and ⑦: modulated outputs by ②, ③ and ④, respectively; ⑧: final time-interleaved output; and ⑨: spectral components of the output normalized by the input peak magnitude). For both cases, ⓐ $= f_c \pm f_s$, ⓑ $= 3f - c \pm f_s$, ⓒ $= 5f - c \pm f_s$, and ⓓ $= 7f - c \pm f_s$.

play important roles in the noise performance of the arrays. An extensive noise analysis is presented in Sections III and IV. Optimization of the duty-cycle and noise filtering technique to relieve the noise issue are proposed in Section IV. The mixer array will be subjected to mismatches between array elements and analytical mismatch models have been provided in Section V. All the theories in the paper have been verified through behavioral mixer simulations including Monte-Carlo statistical simulations in Advance Design System (ADS) [17].

II. Time Interleaved Carrier Modulations

Carrier modulation is fundamentally a multiplication process and Fig. 2(a) shows a typical way of realizing the carrier multiplication relying on the *on-off* switch modulation [18]. The bipolar differential square-wave having 50% duty-cycle, expressed as (1) in the frequency domain, turns *on* each switch differentially per cycle. This will modulate input signal $v_s(t) = V_p sin(2\pi f_s t)$ where $f_s = 1/T_s$. By adding each switch output differentially the final modulated output is illustrated as ③ in the time domain.

$$\Psi_{bc}(f) = \sum_{m=1}^{\infty} \frac{4}{\pi} \frac{sin\left(\frac{m\pi}{2}\right)}{m} e^{-jm\pi/2} \delta(f - mf_c). \quad (1)$$

Equivalently, the input signal will be convoluted by $\Psi_{bc}(f)$ in the frequency domain, resulting in a series of frequency modulation of the input by the fundamental tone and its harmonics of $\Psi_{bc}(f)$. In Fig. 2(a) ④ shows first a few major spectral tones of the modulated output, which are normalized by the peak magnitude of the input: ⓐ $= f_c \pm f_s$, ⓑ $= 3f_c \pm f_s$, ⓒ $= 5f_c \pm f_s$, and ⓓ $= 7f_c \pm f_s$. In typical fundamental mixers, a narrowband filtering will be applied to the output in order to select the fundamentally modulated components shown as ⓐ.

Fig. 2(b) illustrates a time-interleaved (TI) modulation with a time interleaving factor of 3 to realize the same modulation functionality as in Fig. 2(a). In essence the system is a switch array and each switch will be driven by a series of the bipolar square-waves with 50% duty-cycle, called *subcarriers* represented as ②, ③ and ④, respectively. The subcarrier frequency will be reduced by the time-interleaving factor, compared with the fundamental mixer. From the reference of the subcarrier ②, the subcarriers ③ and ④ undergo a successive cumulative delay of T_c. Modulations of input signal by each subcarrier ②, ③ and ④ will output ⑤, ⑥ and ⑦, respectively. An instantaneous combining (or interleaving) of all the outputs gives the final output of ⑧ which contains the same spectral components as in Fig. 2(a).

In general the reference subcarrier ② can be expressed in terms of the fundamental carrier frequency of f_c. This is given

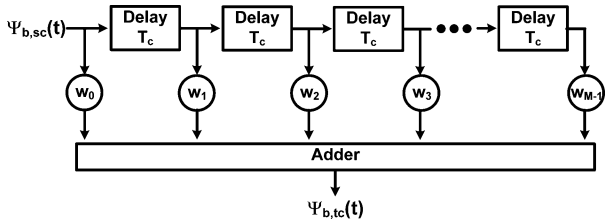

Fig. 3. A transversal filter equivalent to the delay-sum operation in the time-interleaved carrier signal in (3): $w_0 = w_1 = w_2 = w_3 = w_{M-1} = 1$.

as (2) in the frequency domain for an arbitrary *odd* number of the time-interleaving factor M.

$$\Psi_{b,sc}(f) = \sum_{m=-\infty}^{\infty} \frac{4}{\pi} \frac{sin\left(\frac{m\pi}{2}\right)}{m} e^{-jm\pi/2} \delta\left(f - \frac{m}{M} f_c\right), \quad M = odd. \tag{2}$$

Consequently, the summation of total subcarriers will be

$$\begin{aligned}\Psi_{b,tc}(f) &= \sum_{k=0}^{M-1} \Psi_{b,sc}(f)\, e^{-jk2\pi f T_c}, M = odd \\ &= \Psi_{b,sc}(f) \frac{\sin(M\pi f T_c)}{\sin(\pi f T_c)} e^{-j(M-1)\pi f T_c}, f = \frac{mf_c}{M} \\ &= \Psi_{b,sc}(f) \frac{\sin(m\pi)}{\sin\left(\frac{m\pi}{M}\right)} e^{-jm(M-1)\pi/M}, m = M \times odd \\ &= \sum_{n=1}^{\infty} \frac{4}{\pi} \frac{\sin\left(\frac{Mn\pi}{2}\right)}{n} e^{-jMn\pi/2} \delta(f - nf_c). \end{aligned} \tag{3}$$

In (3), $2\pi f T_c$ is a phase delay caused by the time delay of T_c for the subcarriers having f_c/M of frequency. Thanks to the sinusoidal periodicity, it can be shown that $\Psi_{b,tc}(f) = \Psi_{bc}(f)$, and the TI-modulation is a convolution of the input with the $\Psi_{b,tc}(f)$. In the frequency domain, the final modulated output after the interleaving process will be

$$v_{out}(f) = \Psi_{b,tc}(f) \circledast v_s(f) = \Psi_{bc} \circledast v_s(f). \tag{4}$$

Note that under the constraint of 50% duty-cycle in the subcarriers only *odd* number of time interleaving is allowed. The limitation is due to the fact that the time interleaving process is inherently a filtering process: i.e., the term $\sum_{k=0}^{M-1} e^{-jk2\pi f T_c}$ in (3) represents a transfer function from the transversal filter where filter taps have unity weight after a successive time delay of T_c [16]. The transversal filter equivalence in the time domain is shown in Fig. 3 where $w_0 = w_1 = w_2 = w_3 = w_{M-1} = 1$. $\Psi_{b,sc}(t)$ and $\Psi_{b,tc}(t)$ are the time domain representations of $\Psi_{b,sc}(f)$ and $\Psi_{b,tc}(f)$, respectively. The direct-form transversal filter can select (or reject) only the spectral tones comprising $\Psi_{b,sc}(t)$. With 50% duty-cycle, $\Psi_{b,sc}(f)$ in (2) contains fundamental tone of f_c/M and its odd harmonics of mf_c/M $(m = odd)$. Therefore, in order to filter the desired spectral tone of f_c, the length of the transversal filter (or the time-interleaving factor of M) needs to be an *odd* integer larger than 1.

However, if the duty-cycle of the subcarriers is not 50% and if they have a finite DC component, i.e., waveform of the subcarriers is differentially *nonsymmetrical*, then they contain both *even* and *odd* harmonics. These are the cases illustrated as ① and ② in Fig. 4. When considering an arbitrary duty-cycle of

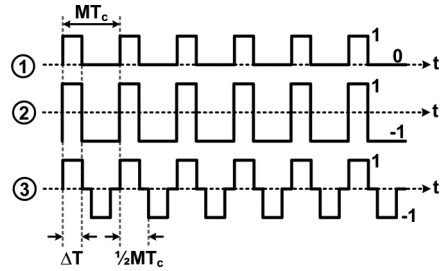

Fig. 4. Rectangular pulse subcarriers (①: a unipolar subcarrier, ②: a non-symmetrical bipolar subcarrier, and ③: an asymmetric bipolar subcarrier).

$\Delta T/(MT_c)$ for the subcarriers where MT_c is a period and ΔT is an active on-time, the waveforms of ① and ② can be expressed as (5) and (6), respectively, in the frequency domain. In these cases spectral components of the subcarriers will be $mf_c/M(m = integer)$, containing both even- and odd-order tones. Therefore, an even length M will also enable to filter the spectral tone of f_c as long as $\Delta T/(MT_c) \neq 50\%$.

$$\Psi_{s,1\,①}(f) = \sum_{m=-\infty}^{\infty} \frac{1}{\pi} \frac{sin\left(m\pi \frac{\Delta T}{MT_c}\right)}{m} \times e^{-jm\pi\Delta T/MT_c} \delta\left(f - \frac{m}{M} f_c\right). \tag{5}$$

$$\Psi_{s,②}(f) = \sum_{m=-\infty}^{\infty} \frac{2}{\pi} \frac{sin\left(m\pi \frac{\Delta T}{MT_c}\right)}{m} \times e^{-jm\pi\Delta T/MT_c} \delta\left(f - \frac{m}{M} f_c\right) - \delta(f). \tag{6}$$

It is worthwhile to note that the *asymmetric* (or *differentially symmetric*) bipolar subcarrier illustrated as ③ in Fig. 4, expressed as (7) in the frequency domain, contains only *odd* harmonics. Thus, only *odd* length of M is allowed to choose the f_c tone.

$$\Psi_{s,③}(f) = \sum_{m=-\infty}^{\infty} \frac{1}{\pi}(1 - cosm\pi) \frac{sin\left(m\pi \frac{\Delta T}{MT_c}\right)}{m} \times e^{-jm\pi\Delta T/MT_c} \delta\left(f - \frac{m}{M} f_c\right). \tag{7}$$

As an example, for the unipolar subcarrier in (5) the final net carrier after M times of interleaving will be given as

$$\begin{aligned}\Psi_{ts,\,①}(f) &= \Psi_{s,\,①}(f) \circledast \mathrm{T}(f) \\ &= \Psi_{s,\,①}(f) \circledast \sum_{\beta=0}^{M-1} e^{-j2\pi f \beta T_c} \\ &= \Psi_{s,\,①}(f) \frac{sin(m\pi)}{sin\left(\frac{m\pi}{M}\right)} e^{-jm(M-1)\pi/M}, \\ & m = integer, \end{aligned} \tag{8}$$

where $T(f) = \sum_{\beta=0}^{M-1} e^{-j2\pi f \beta T_c}$ is the transfer function of the transversal filter in Fig. 3. When $M = 2$, from (5) and (8) it can be found that $\Delta T/(MT_c) = 25\%$ or 75% will give the maximum 2nd -harmonic power, leading to the maximum output power when the input is modulated by the 2nd-harmonic tone. Fig. 5 illustrates the cases of $M = 2$ with 25% and 75% duty-cycles, which essentially represents a behavioral model of the 2x

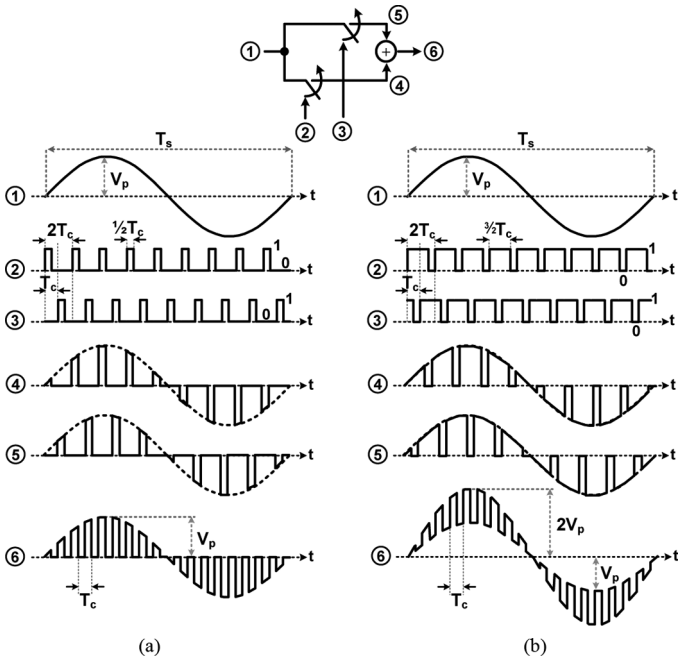

Fig. 5. Time-interleaved carrier modulation with interleaving factor $M = 2$: (a) 25% duty-cycle, (b) 75% duty-cycle.

subharmonic mixer found in many RF applications [19]–[21]. In essence, the 2x and 4x subharmonic mixers [7] can be regarded as subsets of the TI mixer array, corresponding to $M = 2$ and $M = 4$, respectively. For both cases in Fig. 5, the interleaving of ④ and ⑤, which are modulated outputs by the subcarrier ② and ③, respectively, will output the final waveforms of ⑥. The final outputs (Figs. 5(a) and 5(b)) will have the same spectral components as those in Fig. 2 except for the input leakage tone which is modulated by the DC component of the subcarriers. The magnitude of the input leakage to the output will be 3 times larger when the duty-cycle is 75%, because the average total subcarrier power (or DC power) is 3 times larger when $\Delta T/(MT_c) = 75\%$ than when $\Delta T/(MT_c) = 25\%$. The larger carrier power will produce larger output noise, which will be detailed in the next sections.

III. Noise in Carrier Demodulations

Carrier demodulation is a reciprocal process of the carrier modulation, and in general noise is of particular concern in the demodulation process since incoming signal power tends to be weak, susceptible to the system noises in typical wireless communication systems. Consider the abstraction of a single balance mixer shown in Fig. 6(a), which demodulates a modulated signal (presumably an RF signal) and translates the signal frequency, f_s, down to an intermediate frequency of $f_{IF} = f_c - f_s$ (high-side carrier injection). In a typical realization of the carrier demodulator in FET technologies, input voltage signal ($v_s = v_{s,rms} sin\omega_s t$) will be gated to the transconductor ($\mathrm{M_c}$). The transconductor will transform the input signal into a current ($i_s = i_{s,rms} sin\omega_s t$), while generating a noise current ($\overline{i_n}$) as well. For simplification, let's assume the noise current is white Gaussian noise, which will be a reasonable assumption for typical down-conversion mixers. In the single-balanced demodulation, the signal and noise currents will be modulated by the switch pair ($\mathrm{M_{s1,2}}$) driven by the carriers ⓐ and ⓑ, effectively turning the switch pair *on* and *off* alternatively per period. The

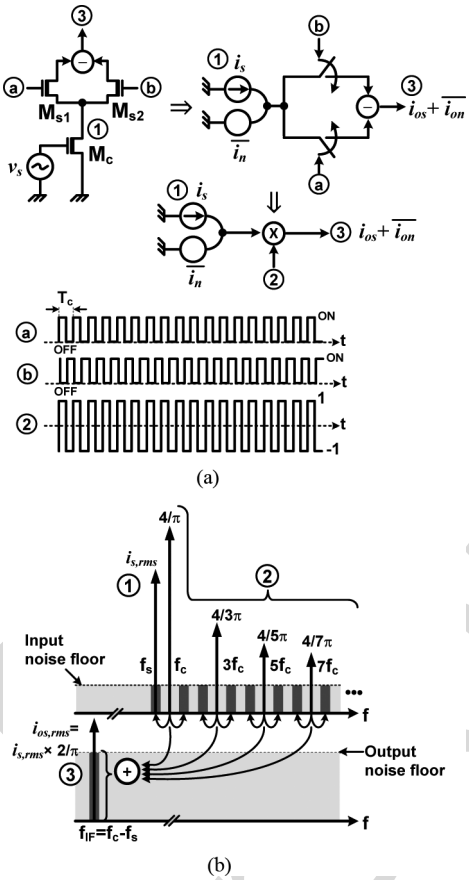

Fig. 6. (a) Single-balanced switching mixer (ⓐ and ⓑ: square-waves turning switch $\mathrm{M_{s1,2}}$ *on* and *off* alternatively, ①: transconductor output signal and noise currents, ②: bipolar square-wave equivalent to the switch *on-off* modulation, and ③: demodulated signal and noise outputs), (b) conceptual description of the signal and noise demodulation in one-sided spectral domain (①: input signal current to the demodulator, ②: spectral tones of the bipolar square-wave, and ③: demodulated signal and noise outputs).

demodulated signal and noise will be taken differentially at the output of ③. The demodulation process is equivalent to modulating the i_s and $\overline{i_n}$ with a unity bipolar carrier illustrated as ② and taking the intermediate output tone.

In the example, the carrier demodulation involves only a half power of the fundamental carrier tone (f_c), and the other half power will contribute to the modulation of the signal to a higher frequency of $f_c + f_s$. In Fig. 6(b) the input noise floor will be set by the transconductor noise $\overline{i_n}$. Assuming 50% duty-ratio in the bipolar pulse train, the carrier contains fundamental and its odd harmonic tones. A uniqueness in the demodulations with rectangular pulse trains is that while signal will be modulated down to a desired IF-band by a tone (usually by a fundamental tone), noise will be modulated by all harmonics as well as by the fundamental tone since the noise is essentially a thermal noise causing a frequency aliasing. This is illustrated in Fig. 6(b) where every noise spectrum distancing $+f_{IF}$ offset (upper sideband) or $-f_{IF}$ offset (lower sideband) from the fundamental tone and its harmonics will be demodulated to the same intermediate frequency as the signal, degrading the SNR at the output.

Because every spectral tone of a carrier pulse will contribute to the noise demodulation, overall power gain factor for the demodulated noise ($G_{pn} = \overline{i_{on}^2}/\overline{i_n^2}$) will be the same as the carrier power, recalling Parseval's power theorem [18]. The carrier waveform and duty-cycle play critical roles in the carrier

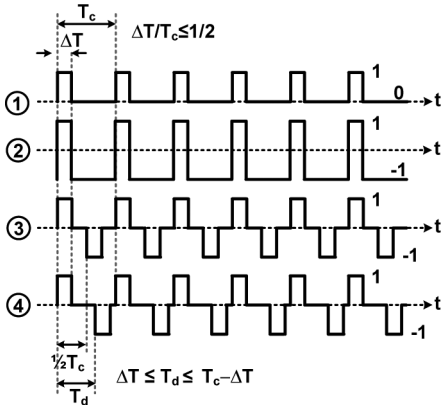

Fig. 7. Rectangular carrier pulses with a duty cycle $\Delta T/T_c \leq 50\%$(T_c: period, ①: $\Psi_{①}(t)$– unipolar pulse, ②: $\Psi_{②}(t)$– nonsymmetrical bipolar pulse, ③: $\Psi_{③}(t)$—asymmetric bipolar differential ($T_d = 1/2T_c$) pulse, and ④:$\Psi_{④}(t)$—asymmetric bipolar pulse with an arbitrary T_d under a constraint of $\Delta T \leq T_d \leq T_c - \Delta T$.

power and therefore in the output SNR. Fig. 7 shows several cases of rectangular carrier pulses with a finite duty-cycle. In the frequency domain each carrier pulse train can be expressed as (9)–(12) at the bottom of the page.

As a practical consideration the duty-cycle is limited to 50%: i.e., $\Delta T/T_c \leq 1/2$. The waveform of ③, $\Psi_{③}(t)$, is a general case of a differential pulse train having a half-period delay in the negative pulse. For a completeness of consideration, the waveform of ④, $\Psi_{④}(t)$, is included and has an arbitrary delay T_d subjected to $\Delta T \leq T_d \leq T_c - \Delta T$ for the negative pulse. $\Psi_{③}(t)$ contains only fundamental tone and its odd harmonics, but introducing T_d $(\neq T_c/2)$ in $\Psi_{④}(t)$ allows even harmonic tones in (12): note $|T_d - T_c/2| \times 2\pi f_c$ represents a differential phase mismatch which induces even harmonics in the *asymmetric* bipolar pulse train. In (12) harmonic power of the m-th tone will be maximized when $T_d/T_c = k/(2m)$ where $k = odd$ and $k/m \leq 1$.

Generally speaking, any harmonic spectral component as well as a fundamental tone in rectangular pulses can be utilized for carrier modulations and demodulations. Table I lists signal power gains ($G_{ps,m} = i^2_{os,rms}/i^2_{s,rms}$) and noise power gains ($G_{pn} = \overline{i^2_{on}}/\overline{i^2_n}$) when they are demodulated by the m-th harmonic tone of each carrier pulse in Fig. 7. The G_{pn} in the table is essentially the carrier power of each carrier type. It should be emphasized that the ratio of $G_{pn}/G_{ps,m}$ addresses a noise factor (NF) [18] of the *demodulation process itself*:

$$\text{Noise Factor} : \mathrm{F}(m) = \frac{(SNR)_{input}}{(SNR)_{output}} = \frac{G_{pn}}{G_{ps,m}}, \tag{13}$$

$$\text{Noise Figure} : \mathrm{NF}(m) = 10 \times log\mathrm{F}(m) = 10 \times log\left(\frac{G_{pn}}{G_{ps,m}}\right). \tag{14}$$

Note that NF is a function of the order of the modulation tone (m) and the carrier duty-cycle. When a carrier demodulation is conducted by a fundamental tone of the unipolar carrier of $\Psi_{①}(t)$ in Fig. 7, then $\Delta T/T_c = 25\%$ and 75% will give the same signal power gain of $G_{ps,1} = 1/(2\pi^2)$, but noise power will be different for each case: $G_{pn} = 1/4$ for $\Delta T/T_c = 25\%$ and $G_{pn} = 3/4$ for $\Delta T/T_c = 75\%$. This results in 3 times larger noise factor in the case with 75% of duty-cycle than the other case: i.e., $\mathrm{F}(1) = \pi^2/2$ for $\Delta T/T_c = 25\%$, and $\mathrm{F}(1) = 3\pi^2/2$ for $\Delta T/T_c = 75\%$. Usually a larger duty-cycle than 50% will worse noise effect and in typical designs the duty-cycle will be limited to 50% to minimize the noise degradation. This is the

---

① : *Unipolar* carrier, $\Psi_{①}(f)$

$$= \sum_{m=-\infty}^{\infty} \frac{1}{\pi} \frac{sin\left(m\pi \frac{\Delta T}{T_c}\right)}{m} e^{-jm\pi\Delta T/T_c} \delta(f - mf_c) \tag{9}$$

② : *Nonsymmetrical* bipolar carrier, $\Psi_{②}(f)$

$$= \sum_{m=-\infty}^{\infty} \frac{2}{\pi} \frac{sin\left(m\pi \frac{\Delta T}{T_c}\right)}{m} e^{-jm\pi\Delta T/T_c} \delta(f - mf_c) - \delta(f) \tag{10}$$

③ : *Asymmetric differential* bipolar carrier, $\Psi_{③}(f)$

$$= \sum_{m=-\infty}^{\infty} \frac{1}{\pi} \frac{sin\left(m\pi \frac{\Delta T}{T_c}\right)}{m} (1 - cosm\pi)\, e^{-jm\pi\Delta T/T_c} \delta(f - mf_c) \tag{11}$$

④ : *Asymmetric* bipolar carrier with a delayT_d, $\Psi_{④}(f)$

$$= \sum_{m=-\infty}^{\infty} \frac{1}{\pi} \frac{sin\left(m\pi \frac{\Delta T}{T_c}\right)}{m} \left(1 - e^{-j2m\pi T_d/T_c}\right) e^{-jm\pi\Delta T/T_c} \delta(f - mf_c),$$

$$where\ \Delta T \leq T_d \leq T_c - \Delta T. \tag{12}$$

TABLE I
SIGNAL POWER GAIN ($G_{\mathrm{ps,m}}$) AND NOISE POWER GAIN (G_{pn}) IN THE DEMODULATION PROCESS BY EACH CARRIER IN FIG. 7.

	$G_{ps,m}$	G_{pn}
①	$\left\{\frac{1}{m\pi}\sin\left(m\pi\frac{\Delta T}{T_c}\right)\right\}^2$	$\frac{\Delta T}{T_c}$
②	$\left\{\frac{2}{m\pi}\sin\left(m\pi\frac{\Delta T}{T_c}\right)\right\}^2$	1
③	$\left\{\frac{1}{m\pi}\sin\left(m\pi\frac{\Delta T}{T_c}\right)\right\}^2 \times(1-\cos m\pi)$	$2\frac{\Delta T}{T_c}$
④	$\left\{\frac{1}{m\pi}\sin\left(m\pi\frac{\Delta T}{T_c}\right) \times\sqrt{2-2\cos\left(2m\pi\frac{T_d}{T_c}\right)}\right\}^2$	$2\frac{\Delta T}{T_c}$

Note: ①, ②, ③, and ④ represent each subcarrier type depicted in Fig. 7, respectively.

main reason for imposing the limitation of $\Delta T/T_c \leq 1/2$ as a practical consideration in this paper.

To verify the theory, behavioral mixer simulations are performed in ADS. Fig. 8 shows results when the fundamental tone ($m = 1$ in the Table I) is utilized for the carrier demodulation. The theoretical NF calculations are based on (14) by applying $G_{ps,m}$ and G_{pn} in Table I, and agreed well with the behavioral simulations. From the Table I, the optimum duty-cycle for maximum signal power gain for all cases can be given as $\Delta T/T_c = k/(2m)$ where $k = odd$ and $k \leq m$: for example, if a fundamental tone ($m = 1$) is utilized for the demodulation, then 50% duty-cycle will give the maximum signal power gain. However, the optimum duty-cycle for maximum SNR is not necessarily coincided with that for the maximum signal power gain. The output SNR will be proportional to $1/\mathrm{F}(m) = G_{ps,m}/G_{pn}$. Therefore, it is apparent from the Table I that, except for the case ②, the optimum duty-cycle minimizing the noise factor can be found as the maximizing (15), resulting in (16) as the condition for the optimum duty-cycle.

$$f\left(\frac{\Delta T}{T_c}\right) = \left\{sin\left(m\pi\frac{\Delta T}{T_c}\right)\right\}^2\left(\frac{\Delta T}{T_c}\right)^{-1},\ where\ \frac{\Delta T}{T_c} \leq \frac{1}{2} \tag{15}$$

$$df\frac{\left(\frac{\Delta T}{T_c}\right)}{d}\left(\frac{\Delta T}{T_c}\right) = 0$$

$$\Rightarrow tan\left(m\pi\left(\frac{\Delta T}{T_c}\right)_{opt}\right)\left(m\pi\left(\frac{\Delta T}{T_c}\right)_{opt}\right)^{-1} = 2$$

$$\Rightarrow m\left(\frac{\Delta T}{T_c}\right)_{opt} \cong 0.371. \tag{16}$$

When $m = 1$, $(\Delta T/T_c)_{opt}$ is about 37.1% which can be confirmed from the behavioral simulation results shown in Figs. 8(a) and 8(c). In general if the m-th harmonic tone of the carrier $\Psi_{①}(t)$ or $\Psi_{③}(t)$ in Fig. 7 is used for a carrier demodulation then the optimum duty-cycle for the maximum SNR will be $(\Delta T/T_c)_{opt} \cong 0.371/m$. For the case of $\Psi_{④}(t)$, noise power is always unity. Therefore, the duty-cycle for the maximum signal power will give the maximum SNR. It is

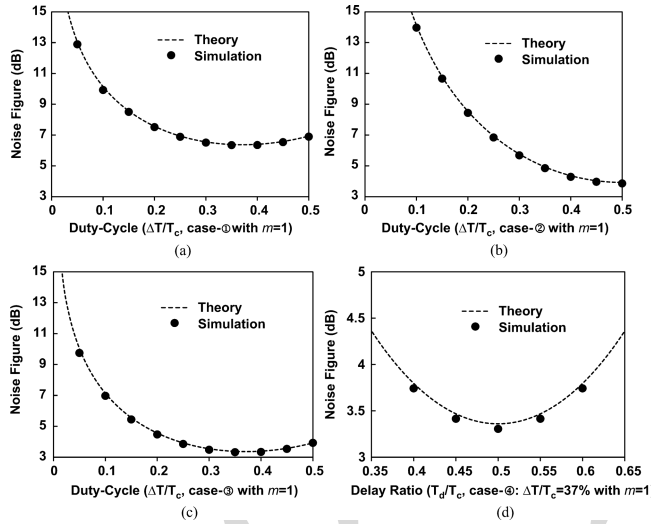

Fig. 8. Noise figure $\mathrm{NF}(m = 1)$ when the fundamental tone of each carrier in Fig. 7 is utilized for the carrier demodulation: (a) $\mathrm{NF}(m = 1)$ with the carrier $\Psi_{①}(t)$, (b) $\mathrm{NF}(m = 1)$ with the carrier $\Psi_{②}(t)$, (c) $\mathrm{NF}(m = 1)$ with the carrier $\Psi_{③}(t)$ and (d) $\mathrm{NF}(m = 1)$ with the carrier $\Psi_{④}(t)$ $(\Delta T/T_c = 37\%)$. Theoretical calculations are based on the expressions of $G_{ps,m}$ and G_{pn} in Table I. Simulations are done based on a behavioral mixer model in ADS.

worthwhile to mention that in a single sideband carrier demodulation based on an ideal sinusoidal multiplication, NF will be 3 dB since noise is populating at double sidebands of a carrier while signal is residing at single sideband. The differential rectangular pulse of $\Psi_{③}(t)$ gives a near optimum NF of 3.36 dB with 37.1% of duty-cycle, as shown in Figs. 8(c) and 8(d).

IV. NOISE IN TIME-INTERLEAVED CARRIER DEMODULATION

A. Correlated and Uncorrelated Noises in Mixer Arrays

Consider two cases of TI-mixer arrays with a time-interleaving factor of M, shown in Fig. 9. In Fig. 9(a) each mixer will be driven by an individual current signal accompanied by a noise current which has no correlation among others, called '*uncorrelated-noise time-interleaved* (UNTI) mixer array'. The array can be transformed equivalently into a single mixer where an equivalent modulation carrier, $\Psi_{\mathrm{oc}}(t)$, can be synthesized by adding all delayed subcarriers of $\Psi_{\mathrm{ic}}(t)$. As discussed, the delay-sum operation of the subcarriers is inherently a filtering process with a transversal filter, which is illustrated in Fig. 10 for various types of subcarrier pulses. In Fig. 9(b) all the signal and noise currents are added before driving mixer array, and therefore each mixer will see the same unified single noise source which behaves like a correlated signal to the mixer array, called '*correlated-noise time-interleaved* (CNTI) mixer array'. The coherent signal currents are added linearly in current domain, increasing their magnitude by a factor of $\sqrt{M}$. But the uncorrelated noises will be added in power domain, effectively increasing their *rms* magnitude by a factor of in Fig. 9(b). In terms of the signal currents there is no difference between the two array topologies, and in the frequency domain the output signal will be

$$i_{os}(f) = i_s(f) \circledast \Psi_{ic} \circledast \mathrm{T}(f). \tag{17}$$

, where $\mathrm{T}(f)$ is the transfer function of the transversal filter given in (8). In view of noise, however, each mixer in the UNTI-mixer array will be driven by an *uncorrelated*

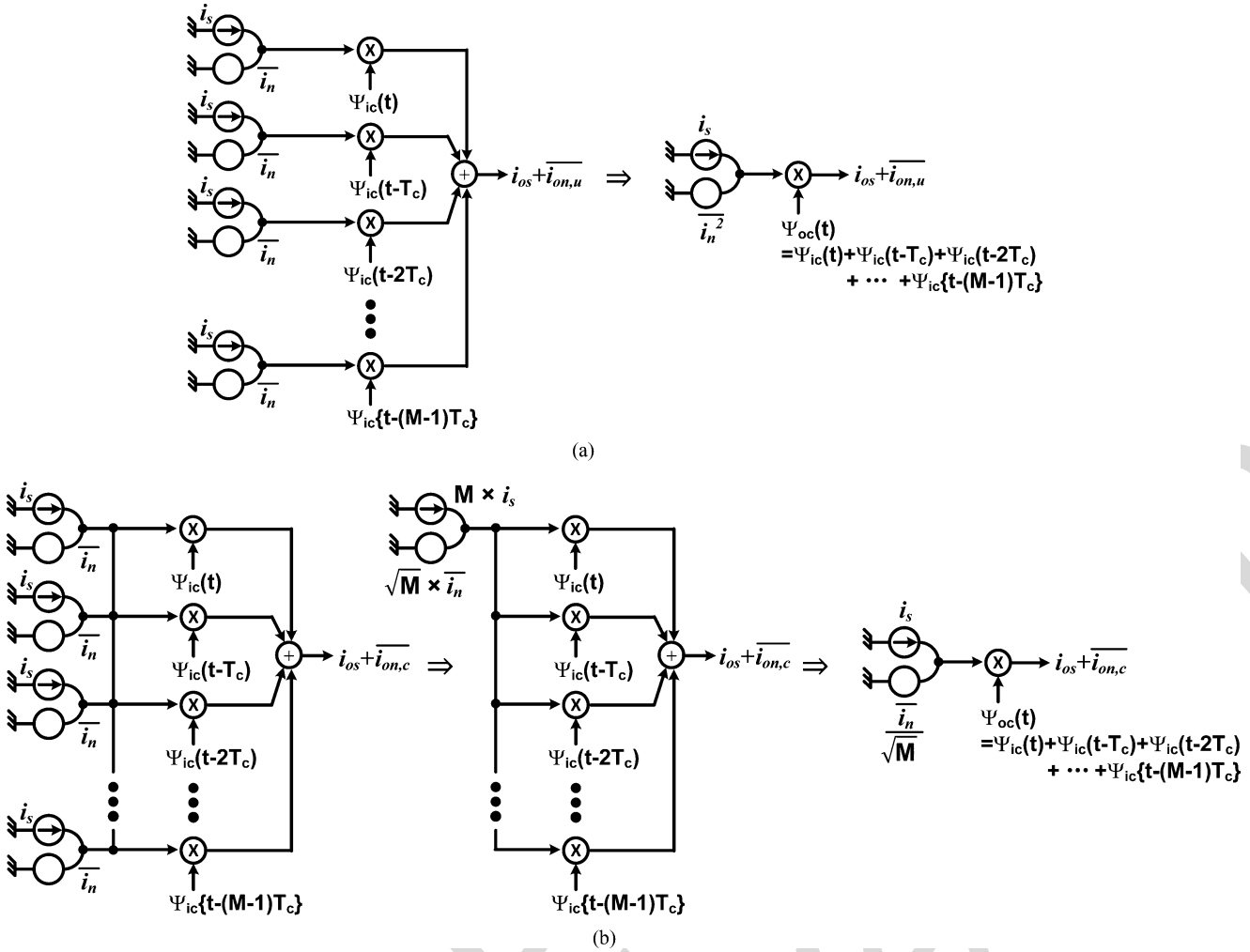

Fig. 9. Time-interleaved carrier modulation/demodulation with a time interleaving factor of M: (a) time-interleaved mixer array with uncorrelated noises to each mixer (UNTI-mixer array), (b) time-interleaved mixer array with correlated noises to each mixer (CNTI-mixer array).

noise and the net result is that all the subcarriers' fundamental and harmonic tones will involve in the noise demodulation. This effectively increases output noise power by a factor of the time-interleaving factor as expressed in (18). In the CNTI-mixer array in Fig. 9(b), each mixer is driven by a correlated noise. Therefore, only the subcarriers' spectral tones which are filtered in through the transversal filter will participate in the noise demodulation, which is expressed mathematically in (19).

$$\begin{aligned}
\overline{i_{on,u}(f)} &= \overline{i_n(f)} \circledast \Psi_{oc}(f) = \overline{i_n(f)} \circledast \Psi_{ic}(f)\,\mathrm{T}(f) \\
&\Rightarrow \overline{i_{on,u}{}^2(f)} = \overline{i_{on,u}(f)\, i_{on,u}(f)^*} \\
&= \overline{i_n{}^2} \circledast |\Psi_{ic}(f)|^2 \times M \\
&\Rightarrow G_{pn,u} = \frac{\overline{i_{on,u}{}^2(f)}}{\overline{i_n{}^2}} \\
&= M \times \sum_{m=-\infty}^{\infty} \left|\Psi_{ic}\left(\frac{m}{M} f_c\right)\right|^2 \qquad (18)
\end{aligned}$$

$$\begin{aligned}
\overline{i_{on,c}(f)} &= \frac{\overline{i_n(f)}}{\sqrt{M}} \circledast \Psi_{oc}(f) = \frac{\overline{i_n(f)}}{\sqrt{M}} \circledast \Psi_{ic}(f) \circledast \mathrm{T}(f) \\
&\Rightarrow \overline{i_{on,c}{}^2(f)} = \overline{i_{on,c}(f)\, i_{on,c}(f)^*} \\
&= \frac{\overline{i_n{}^2}}{M} \circledast \left|\Psi_{ic}\left(\frac{m}{M} f_c\right) \frac{sin(m\pi)}{sin\left(\frac{m\pi}{M}\right)}\right|^2 \\
&\Rightarrow G_{pn,c} = \frac{\overline{i_{on,c}{}^2(f)}}{\overline{i_n{}^2}} \\
&= \sum_{m=-\infty}^{\infty} \frac{1}{M} \left|\Psi_{ic}\left(\frac{m}{M} f_c\right) \frac{sin(m\pi)}{sin\left(\frac{m\pi}{M}\right)}\right|^2. \qquad (19)
\end{aligned}$$

In (18) and (19), $G_{pn,u}$ and $G_{pn,c}$ mean *uncorrelated* noise power gain and *correlated* noise power gain in each UNTI- and CNTI-mixer array, respectively. A net difference between the *correlated* and *uncorrelated* noises in TI-mixer arrays is that the *uncorrelated* noise will be added linearly versus the transversal filter length (or mixer array length) of M, while the *correlated* noise will be shaped by the transversal filter.

B. Duty-Cycle Control

In the TI-mixer arrays with M times of interleaving, the demodulation process relies on the M-th harmonic tone of the subcarrier spectrum. For each case of the subcarrier type illustrated in Fig. 10, Table II shows signal power gain and noise power gains for both cases of UNTI- and CNTI-mixer arrays.

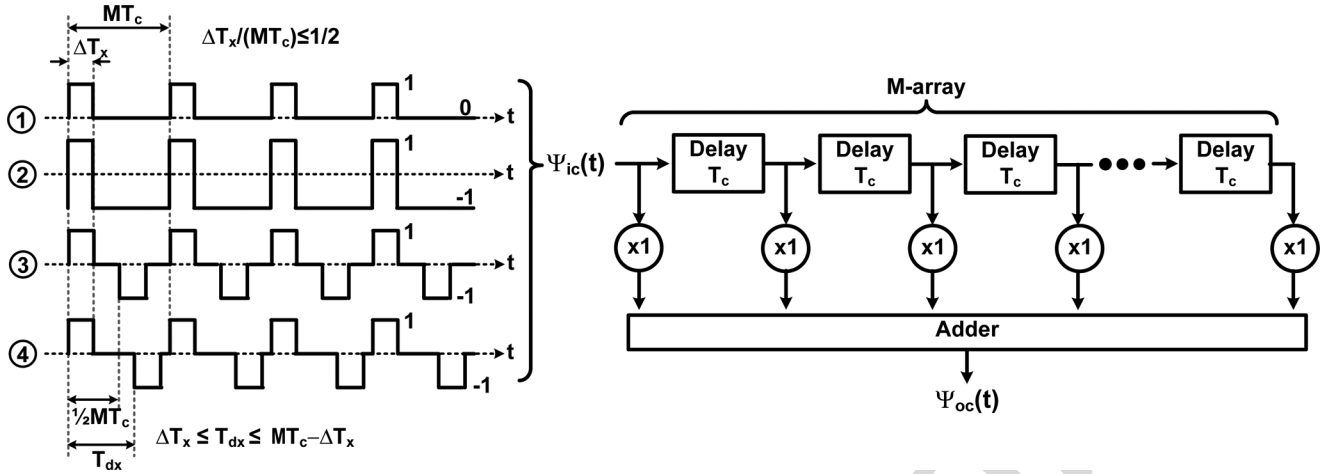

Fig. 10. Filtering rectangular carrier pulses using a transversal filter which is equivalent to the carrier synthesis based on the delay-sum operation in time-interleaved mixer arrays with M of time interleaving factor. ①: $\Psi_{s,①}(t)$- unipolar subcarrier pulse, ②: $\Psi_{s,②}(t)$- nonsymmetrical bipolar subcarrier pulse, ③: $\Psi_{s,③}(t)$—asymmetric bipolar differential ($\mathrm{T_dx} = 1/2\mathrm{MT_c}$ subcarrier pulse, and ④: $\Psi_{s,④}(t)$—asymmetric bipolar subcarrier pulse with an arbitrary T_{dx} under a constraint of $\Delta\mathrm{T_x} \leq \mathrm{T_{dx}} \leq \mathrm{MT_c} - \Delta\mathrm{T_x}$.

$G_{ps,m}$ is signal power gain when the demodulation is conducted by the m-th harmonic tone of the subcarriers. Because of a perfect correlation among the noises, noise power gain in the CNTI-mixer array ($G_{pn,c}$ in Table II) can be expressed in terms of the signal power gain, $G_{pn,c}$, which can be much smaller than that $G_{pn,u}$ from the UNTI-mixer array. The term $(\sin m\pi / \sin m\pi/M)^2$ in $G_{ps,m}$ and $G_{pn,c}$ comes from the harmonic filtering function of the transversal filter inherited in the mixer array. The theoretical power gains in Table II have been verified through behavioral mixer array simulations in ADS, and typical results for $M = 3$ are shown in Fig. 11. $G_{ps,m}$ and $G_{pn,c}$ have a periodicity associated with the sinusoidal periodicity in $\sin(3\pi \times duty - cycle)$. Noise performance in the mixer arrays can be optimized by engineering duty-cycle of each subcarrier pulse. For UNTI-mixer arrays, with the same logics applied in (15), the optimum duty-cycle minimizing NF for each of the $\Psi_{s,①}(t)$, $\Psi_{s,}(t)$ and $\Psi_{s,}(t)$ in Fig. 10 can be found as

$$\left(\frac{\Delta T_x}{MT_c}\right)_{opt} \cong \frac{0.371}{\mathrm{m}}. \quad (20)$$

If a three-mixer array is used to utilize the 3rd-harmonic tone $(m = 3)$ of the subcarrier for demodulations, then the optimum duty-cycle will be $0.371/3 = 12.4\%$, which can be seen in the results shown in Figs. 11(a) and 11(c). As in fundamental mixers, a fully differential subcarrier (Fig. 11(c)) will exhibit the best SNR performance compared with the other types of subcarrier. For the differential subcarrier, 50% of duty-cycle is near optimum to get the maximum SNR. Note that in the time-interleaving technique with the differential subcarrier, signal power gain in the CNTI-mixer array can be larger than noise power gain. This process gain comes from the array configuration where by adding coherent signals and random noises before mixer arrays, effective SNR can be increased by the factor of the array length M, when compared with the SNR in a single mixer. From Fig. 11, it can also be confirmed that the SNR performance in the CNTI-array will be superior to that in the UNTI-array.

C. Noise Filtering

The optimization of duty-cycle to maximize SNR could be an economic solution for low frequency applications. However, it

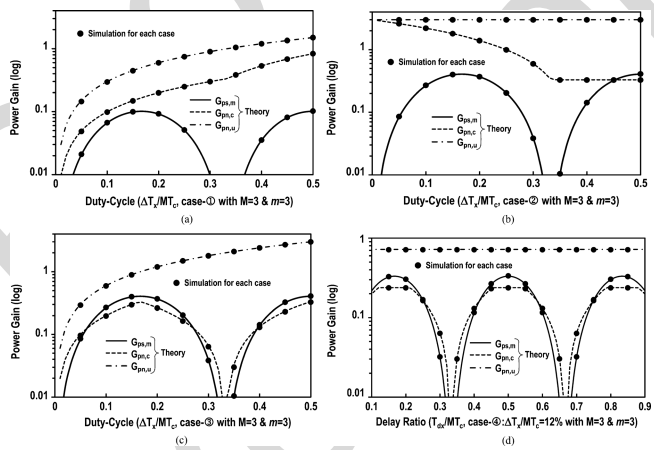

Fig. 11. Signal power gain, correlated noise power gain, and uncorrelated noise power gain for a 3-mixer array ($M = 3$) with various types of subcarriers described in Fig. 10(a) case with the unipolar subcarrier $\Psi_{s,}(t)$ case with the nonsymmetrical bipolar subcarrier $\Psi_{s,}(t)$, (c) case with the asymmetric differential bipolar subcarrier $\Psi_{s,}(t)$ and (d) case with the asymmetric bipolar subcarrier $\Psi_{s,}(t)$ with an arbitrary delay of $\mathrm{T_{dx}}$. Theoretical calculations are based on the expressions of $G_{ps,m}$ and $G_{pn,u}$ in Table II. Simulations are done based on a behavioral mixer model in ADS.

will be a challenging task to control the duty-cycle with a high accuracy at high frequencies, such as RF, microwave and millimeter-wave carrier modulations. As an alternative approach to the duty-cycle control, noise can be filtered out before the TI-demodulator arrays. A noise filter can be realized with an affordable manner at high frequencies using passive components.

1) Bandpass Noise Filtering: Consider applying an ideal bandpass filtering to each TI-mixer array configuration in Fig. 9, which is illustrated in Fig. 12. To simplify discussion, let's assume that the bandpass filter (BPF) has a finite bandwidth (BW) extending over $f_s \pm 2f_{IF}$ centered at f_s. Suppose the demodulation is conducted by an ideal differential rectangular *subcarrier* of $\Psi_{s,③}(t)$ in Fig. 10 which has 50% duty-cycle with a fundamental frequency of $f_{c,sub} = (f_s + f_{IF})/M$. If the filter BW is smaller than $2 \times f_{c,sub}$, then the noise spectrum will not be aliased and the demodulation process will be equivalent to an ideal sinusoidal multiplication process. In such scenario, the M-th harmonic of $f_{c,sub} (= Mf_{c,sub} = f_s + f_{IF})$

TABLE II
SIGNAL POWER GAIN ($G_{\mathrm{ps,m}}$) AND NOISE POWER GAIN (G_{pn}) IN THE TIME-INTERLEAVED DEMODULATION PROCESS PERFORMED BY EACH CARRIER IN FIG. 10.

	$\mathbf{G_{ps,m}}$	$\mathbf{G_{pn,u}}$	$\mathbf{G_{pn,c}}$
①	$\left\{\frac{1}{m\pi}\sin\left(m\pi\frac{\Delta T_x}{MT_c}\right)\right\}^2\left(\frac{\sin m\pi}{\sin\frac{m\pi}{M}}\right)^2$	$\frac{\Delta T_x}{MT_c}\times M=\frac{\Delta T_x}{T_c}$	$\frac{1}{M}\sum_{m=-\infty}^{\infty}\left\{\frac{1}{m\pi}\sin\left(m\pi\frac{\Delta T_x}{MT_c}\right)\right\}^2\left(\frac{\sin m\pi}{\sin\frac{m\pi}{M}}\right)^2$
②	$\left\{\frac{2}{m\pi}\sin\left(m\pi\frac{\Delta T_x}{MT_c}\right)\right\}^2\left(\frac{\sin m\pi}{\sin\frac{m\pi}{M}}\right)^2$	M	$M\left(2\frac{\Delta T_x}{MT_c}-1\right)^2+\frac{2}{M}\sum_{m=1}^{\infty}\left\{\frac{2}{m\pi}\sin\left(m\pi\frac{\Delta T_x}{MT_c}\right)\right\}^2\left(\frac{\sin m\pi}{\sin\frac{m\pi}{M}}\right)^2$
③	$\left\{\frac{1}{m\pi}\sin\left(m\pi\frac{\Delta T_x}{MT_c}\right)\times(1-\cos m\pi)\right\}^2\left(\frac{\sin m\pi}{\sin\frac{m\pi}{M}}\right)^2$	$2\frac{\Delta T_x}{MT_c}\times M=2\frac{\Delta T_x}{T_c}$	$\frac{1}{M}\sum_{m=-\infty}^{\infty}\left\{\frac{1}{m\pi}\sin\left(m\pi\frac{\Delta T_x}{MT_c}\right)\times(1-\cos m\pi)\right\}^2\left(\frac{\sin m\pi}{\sin\frac{m\pi}{M}}\right)^2$
④	$\left\{\frac{\frac{1}{m\pi}\sin\left(m\pi\frac{\Delta T_x}{MT_c}\right)}{\times\sqrt{2-2\cos\left(2m\pi\frac{T_{dx}}{MT_c}\right)}}\right\}^2\left(\frac{\sin m\pi}{\sin\frac{m\pi}{M}}\right)^2$	$2\frac{\Delta T_x}{MT_c}\times M=2\frac{\Delta T_x}{T_c}$	$\frac{1}{M}\sum_{m=-\infty}^{\infty}\left\{\frac{\frac{1}{m\pi}\sin\left(m\pi\frac{\Delta T_x}{MT_c}\right)}{\times\sqrt{2-2\cos\left(2m\pi\frac{T_{dx}}{MT_c}\right)}}\right\}^2\left(\frac{\sin m\pi}{\sin\frac{m\pi}{M}}\right)^2$

***Note: ①, ②, ③, and ④ represent each subcarrier type depicted in Fig. 10, respectively.**

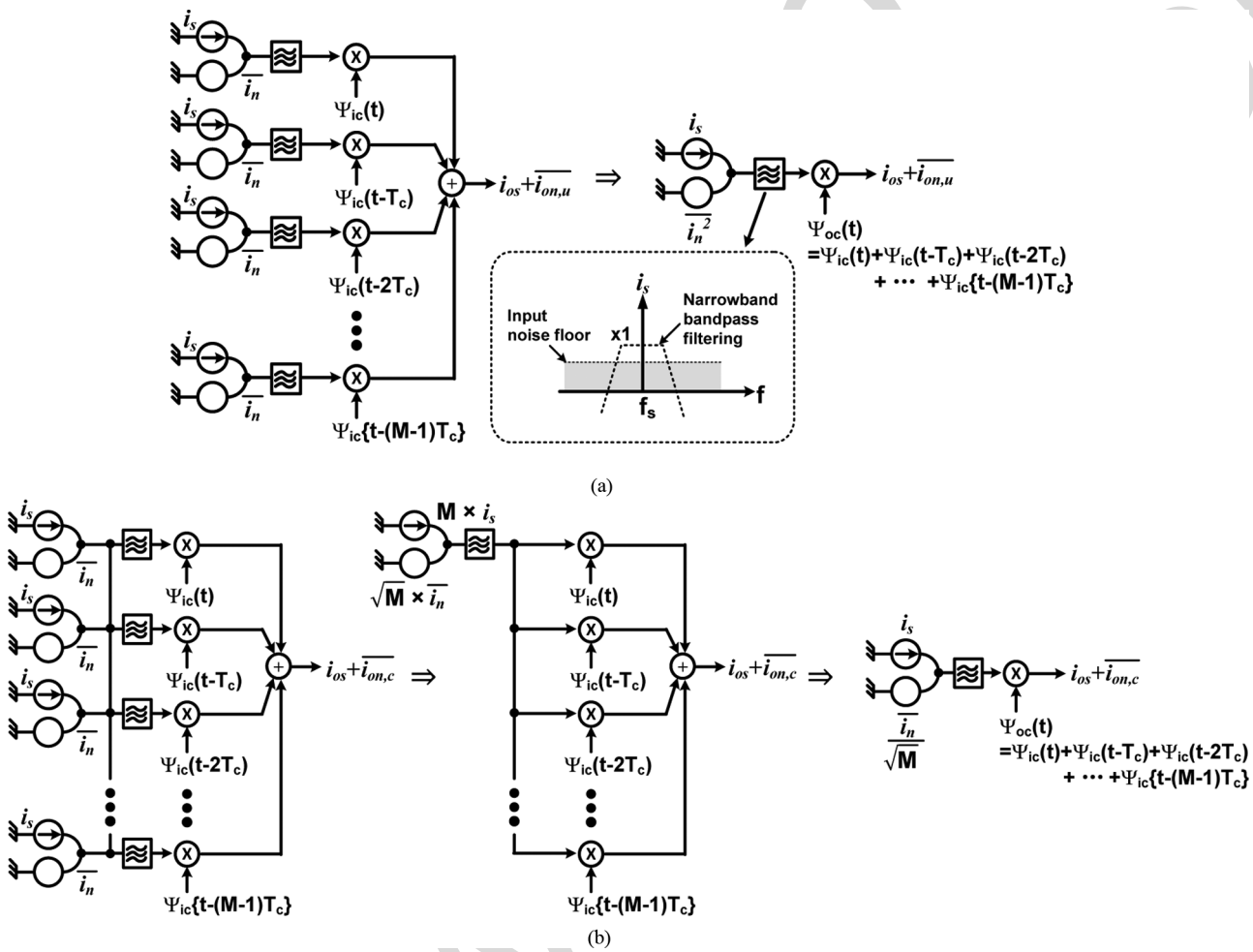

Fig. 12. Noise filtering in time-interleaved carrier modulations and demodulations: (a) time-interleaved demodulator array with filtering uncorrelated noises, (b) time-interleaved demodulator array with filtering correlated noises.

will demodulate the signal and noise. Output signal power gain will be $(2/\pi)^2$ for both cases UNTI- and CNTI-mixer arrays in Fig. 12. In view of noise the *uncorrelated* noise power gain in Fig. 12(a), given as $G_{pn,u} = \overline{i_{on,u}^2}/\overline{i_n^2} = (2/\pi)^2 \times M$, will be the same as the *correlated* noise power gain in Fig. 12(b) given as $G_{pn,c} = \overline{i_{on,c}^2}/\overline{i_n^2} = (2M/\pi)^2 \times 1/M$. When an ideal band-pass filtering is applied, the UNTI-mixer array will exhibit the same SNR as in the CNTI-mixer array. In real implementations, the BPF can be realized as a tuned load of RF front-end circuitry (e.g., LNAs) proceeding the mixer array.

2) Highpass Noise Filtering: While the BPF playing as an antialiasing noise filter guarantees an optimum output SNR in

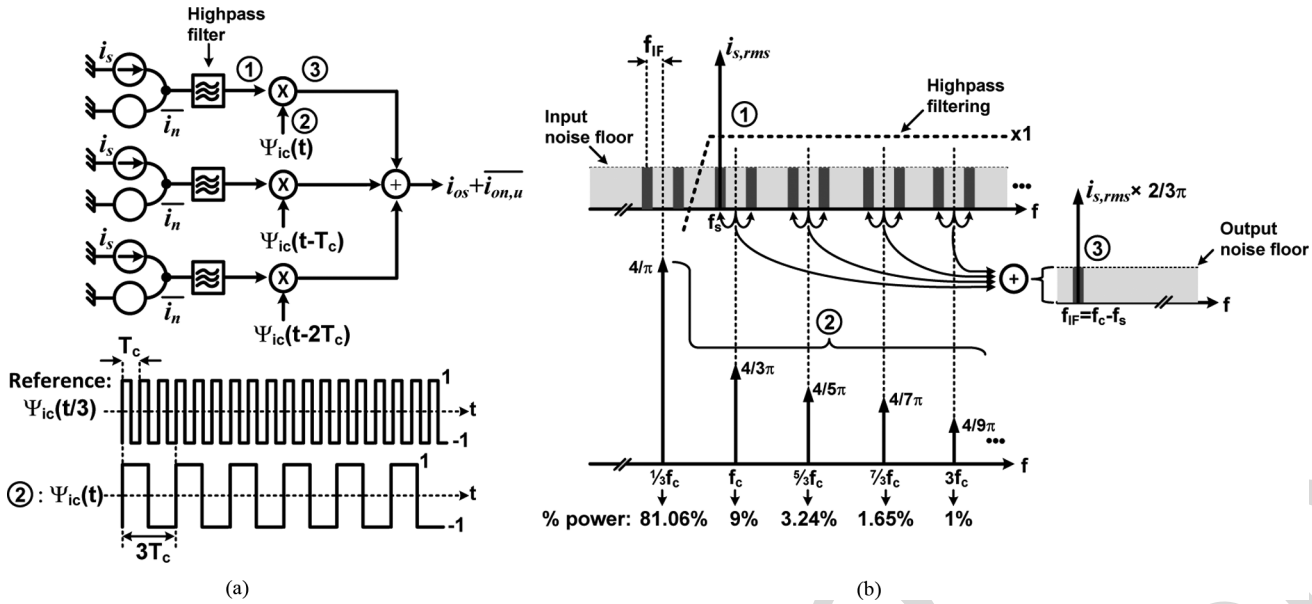

Fig. 13. (a) Noise filtering around fundamental frequency of the *subcarrier* $\Psi_{\rm ic}(t)$ with a highpass filter in time-interleaved mixer array with a time interleaving factor $M = 3$, (b) conceptual description of spectral tones in the single path of the array.

TABLE III
SIGNAL POWER GAIN ($G_{\rm ps,m}$) AND NOISE POWER GAIN ($G_{\rm pn,u}$) AFTER HIGH-PASS NOISE FILTERING IN THE TIME-INTERLEAVED DEMODULATION PROCESS PERFORMED BY EACH CARRIER IN FIG. 10.

	$G_{\rm pn,u}$	$G_{\rm pn,c}$
①	$\left(\frac{\Delta T_x}{MT_c}-\left(\frac{\Delta T_x}{MT_c}\right)^2-2\sum_{k=1}^{M-1}\left\{(1-\delta_k{}^2)\left(\frac{1}{k\pi}\sin\left(k\pi\frac{\Delta T_x}{MT_c}\right)\right)^2\right\}\right)\times M$	$\frac{2}{M}\sum_{m=1}^{\infty}\left\{\frac{1}{m\pi}\sin\left(m\pi\frac{\Delta T_x}{MT_c}\right)\right\}^2\left(\frac{\sin m\pi}{\sin\frac{m\pi}{M}}\right)^2$
②	$\left(1-\left(1-\frac{2\Delta T_x}{MT_c}\right)^2-2\sum_{k=1}^{M-1}\left\{(1-\delta_k{}^2)\left(\frac{2}{k\pi}\sin\left(k\pi\frac{\Delta T_x}{MT_c}\right)\right)^2\right\}\right)\times M$	$\frac{2}{M}\sum_{m=1}^{\infty}\left\{\frac{2}{m\pi}\sin\left(m\pi\frac{\Delta T_x}{MT_c}\right)\right\}^2\left(\frac{\sin m\pi}{\sin\frac{m\pi}{M}}\right)^2$
③	$2\left(\frac{\Delta T_x}{MT_c}-\sum_{k=1}^{M-1}\left\{(1-\delta_k{}^2)\left(\frac{1}{k\pi}\sin\left(k\pi\frac{\Delta T_x}{MT_c}\right)\right)^2\times(1-\cos k\pi)\right\}\right)\times M$	$\frac{1}{M}\sum_{m=-\infty}^{\infty}\left\{\frac{1}{m\pi}\sin\left(m\pi\frac{\Delta T_x}{MT_c}\right)\right\}^2\times(1-\cos m\pi)\left(\frac{\sin m\pi}{\sin\frac{m\pi}{M}}\right)^2$
④	$2\left(\frac{\Delta T_x}{MT_c}-\sum_{k=1}^{M-1}\left\{(1-\delta_k{}^2)\left(\frac{\frac{1}{k\pi}\sin\left(k\pi\frac{\Delta T_x}{MT_c}\right)}{\sqrt{2-2\cos\left(2k\pi\frac{T_{dx}}{MT_c}\right)}}\right)^2\right\}\right)\times M$	$\frac{1}{M}\sum_{m=-\infty}^{\infty}\left\{\frac{\frac{1}{m\pi}\sin\left(m\pi\frac{\Delta T_x}{MT_c}\right)}{\sqrt{2-2\cos\left(2m\pi\frac{T_{dx}}{MT_c}\right)}}\right\}^2\left(\frac{\sin m\pi}{\sin\frac{m\pi}{M}}\right)^2$

***Note: ①, ②, ③, and ④ represent each subcarrier type depicted in Fig. 10, respectively.**

the TI-mixer array, highpass filter (HPF) can also improve the noise performance significantly in the UNTI-mixer arrays. This is illustrated conceptually in Fig. 13 for the case of $M = 3$ with an ideal differential rectangular subcarrier having 50% duty-cycle. Assuming a narrow IF-band in the array shown in Fig. 13(a), only the 3rd-harmonic tone (f_c) of the subcarrier $\Psi_{\rm ic}(t)$ demodulates signal to the IF-band and all the other tones involves noise aliasing. Noise modulation by the fundamental tone $(1/3f_c)$ of the subcarrier accounts for about 81% of total output noise power as illustrated in Fig. 13(b). Therefore, an ideal filtering out the noise around the fundamental tone by a HPF will improve the output SNR by 81%. The HPF will also reject DC noise in CNTI-array with unipolar subcarriers, reducing noise factor. However, for CNTI-array with bipolar differential subcarriers, the *correlated* noises around the fundamental tone will be filtered out already by the transversal filter inherited in the mixer array in ideal operation and extra filtering by the HPF will not improve the noise performance.

In general M-array with *uncorrelated* noises, noises residing lower sideband of the M-th harmonic tone of a subcarrier can be rejected by a HPF. Table III summarizes *correlated* and *uncorrelated* noise power gain after the highpass noise filtering when driven by different types of the subcarrier. In Table III, $(\Delta T_x/(MT_c))^2$ and $(1-2\Delta T_x/(MT_c))^2$ are the rejected DC powers by the HPFs when the array is driven by the subcarrier $\Psi_{\rm s,④}(t)$ and $\Psi_{\rm s,②}(t)$ in Fig. 10, respectively. In the table, δ_k ($k = 1$ to $M-1$) expresses finite rejection ratio of the k-th harmonic tone by the HPF: for example, $\delta_1 = 0.1$ means -20 dB of rejection for the fundamental tone $(= f_c/M)$ of the subcarrier.

The gain expressions in Table III have been verified with behavioral TI-mixer array simulations in ADS. Typical simulation results for $M = 3$ with the various types of subcarrier

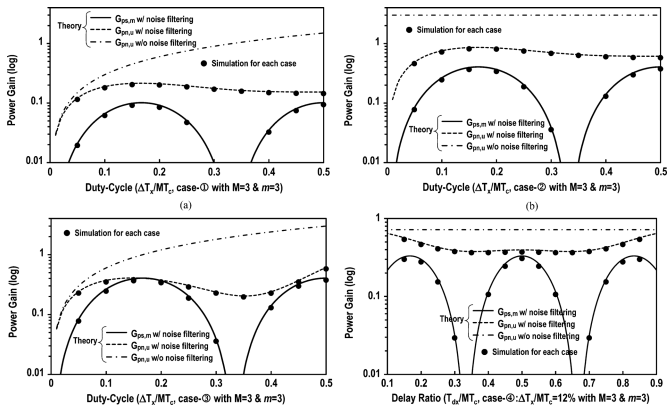

Fig. 14. Signal power gain and uncorrelated noise power gain after a highpass noise filtering for 3-mixer array ($M = 3$) with various types of subcarriers described in Fig. 10: (a) case with the unipolar subcarrier $\Psi_{s,}(t)$, (b) case with the nonsymmetrical bipolar subcarrier $\Psi_{s,}(t)$, (c) case with the asymmetric differential bipolar subcarrier $\Psi_{s,}(t)$, and (d) case with the asymmetric bipolar subcarrier $\Psi_{s,}(t)$ with an arbitrary delay of $\mathrm{T_{dx}}$. Theoretical calculations are based on the expressions of $G_{ps,m}$ and $G_{pn,u}$ in Table III. Simulations are done based on a behavioral mixer model in ADS.

depicted in Fig. 10 are shown in Fig. 14. The 3rd-order Butterworth-type HPF has been utilized in the behavioral simulations for the highpass noise filtering. In the simulation set-up, the signal frequency is $f_s = 120$ GHz, and the fundamental frequency of subcarrier is $f_c/M = 41$ GHz, resulting in $f_{IF} = 3$ GHz. The filter cut-off frequency is about 80 GHz, around the 2nd-harmonic tone of the subcarrier. Under the filter response, $\delta_1 = 0.134$ and $\delta_2 = 0.734$, which will reject about 98% and 46% of the fundamental noise power and the second-harmonic noise power, respectively, with a minimal loss for the signal. In Fig. 14, the theoretical $G_{pn,u}$ without noise filtering is also displayed together for a comparison purpose. There is a good agreement between the theory and behavioral simulation results. For every case, output noise power can be reduced by an order of magnitude with the noise filtering, while maintaining 50% of duty-cycle.

Finally, it is worthwhile to mention that the linearity performance, e.g., the 3rd order input intercept point ($\mathrm{IIP_3}$) or -1 dB gain compression point ($P_{-1\,\mathrm{dB}}$), of the mixer array would be better than a single mixer, assuming that the linearity performance of each individual mixer element in the array are the same as that of the single mixer. For instance, in the M-array the ($\mathrm{IIP_3}$) of the mixer array will be $10\log M$ higher than the IIP3 of single mixer. This is because that in the M-element array, the effective input power for individual mixer will be M times smaller than the input power of the single mixer [22].

V. Error Analysis

A. Mismatch Analysis

Fig. 15 illustrates the array experiencing random gain mismatches and delay mismatches among the elements. $\Delta T_{\epsilon,\mathrm{n}}$ ($n = 1$ to $\mathrm{M}-1$) represents delay mismatch in each subcarrier from the reference subcarrier of $\Psi_{\mathrm{ic}}(t)$ shown as ①$\Delta w_{\epsilon,\mathrm{n}}$ ($n = 1$ to M-1) expresses gain mismatch in each array path with reference to the path gain which is modulated by the subcarrier ①. The random mismatches can be addressed as errors in the filter coefficients in the transversal filter. The gain mismatches are equivalently expressed as amplitude mismatches among the subcarriers. The $\Delta T_{\epsilon,n}$ and $\Delta w_{\epsilon,n}$ will originate from a device mismatch which is usually a random process having Gaussian statistics in electronics. Therefore, the $\Delta T_{\epsilon,n}$ and $\Delta w_{\epsilon,\mathrm{n}}$ can be treated as Gaussian random variables. Strictly speaking, they are independent among the array elements, requiring a joint probability of multiple random variables to describe the mismatch behavior in the TI-mixer array [23].

To simplify the discussion and to estimate the error in first order, following assumptions can be made. First, in real implementation a unit mixer will be repeated to form the mixer array, which means the $\Delta \mathrm{w}_{\epsilon,n}$ will have an equal 1σ-variance that can be expressed as $\overline{W_\varepsilon}$. In incorporating a successive delay in the subcarriers, an identical unit delay element can be cascaded and the variance of $\Delta T_{\epsilon,n}$ will be same in each delay element, which can be represented as $\overline{\tau_\varepsilon}$. The worst case scenario will be that the $\Delta w_{\epsilon,n}$ and $\Delta T_{\epsilon,n}$ have a perfect correlation among the mixer elements and the delay cells. In the worst case scenario, the variance of $\Delta T_{\epsilon,n}$ will be accumulated linearly when propagating the delay chain in Fig. 15. These assumptions are reflected in the transversal filter transfer function, $\mathrm{T}_\varepsilon(f)$ in (21) at the bottom of the following page, where the mismatch random variables are incorporated in the complex weights in the first step and then each random variable is approximated to its 1σ-variance. Note, $\overline{W_\varepsilon}$ and $\overline{\tau_\varepsilon}$ can be treated as another Gaussian random variables which are common to each mixer and delay element. $\overline{W_\varepsilon}$ and $\overline{\tau_\varepsilon}$ will have the same statistical properties as $\Delta w_{\epsilon,n}$ and $\Delta T_{\epsilon,\mathrm{n}}$, respectively.

Usually the random mismatches are weak perturbations and it will be a reasonable assumption that $1 \gg \overline{\tau_\varepsilon}/T_c$. This allows $e^{-jm\pi(1+\overline{\tau_\varepsilon}/T_c)} \cong e^{-jm\pi} = cosm\pi$ in (21), resulting in the approximation of the magnitude response of the transversal filter transfer function as

$$|\mathrm{T}_\varepsilon(f)| = |\mathrm{T}_\varepsilon\left(\frac{m}{MT_c}\right)|, m = integer$$
$$\cong 1 + \left(1+\overline{W_\varepsilon}\right)\cos m\pi \left(\frac{\sin\left(\frac{m\pi}{M}\left(1+\frac{\overline{\tau_\varepsilon}}{T_c}\right)(M-1)\right)}{\sin\left(\frac{m\pi}{M}(1+\frac{\overline{\tau_\varepsilon}}{T_c})\right)}\right). \quad (22)$$

The output signal, $i_{os,\varepsilon}(f)$, under the finite mismatches in the array will be

$$i_{os,\varepsilon}(f) = i_s(f)\,\Psi_{ic}(f)\,\mathrm{T}_\varepsilon(f). \quad (23)$$

The signal power gain $G_{ps,m}$ under the mismatches can be found by replacing $(\sin m\pi/\sin m\pi/M)^2$ with $|\mathrm{T}_\varepsilon(f)|^2$ in Table II and Table III. The *uncorrelated* noise power gain under the mismatches in UNTI-mixer arrays, $G_{pn,u\varepsilon}$ corresponding to $G_{pn,u}$ in (18), can be given as

$$\frac{\overline{i_{on,u\varepsilon}(f)} = \overline{i_n(f)\Psi_{ic}(f)\,\mathrm{T}_\varepsilon(f)}}{\overline{i_{on,u\varepsilon}{}^2(f)} = \overline{i_{on,u\varepsilon}(f)\,i_{on,u\varepsilon}(f)^*}}$$
$$= \overline{i_n{}^2}|\Psi_{ic}(f)|^2\left\{1 + \sum_{\beta=1}^{M-1}\left(1+\overline{W_\varepsilon}\right)^2\right\}$$

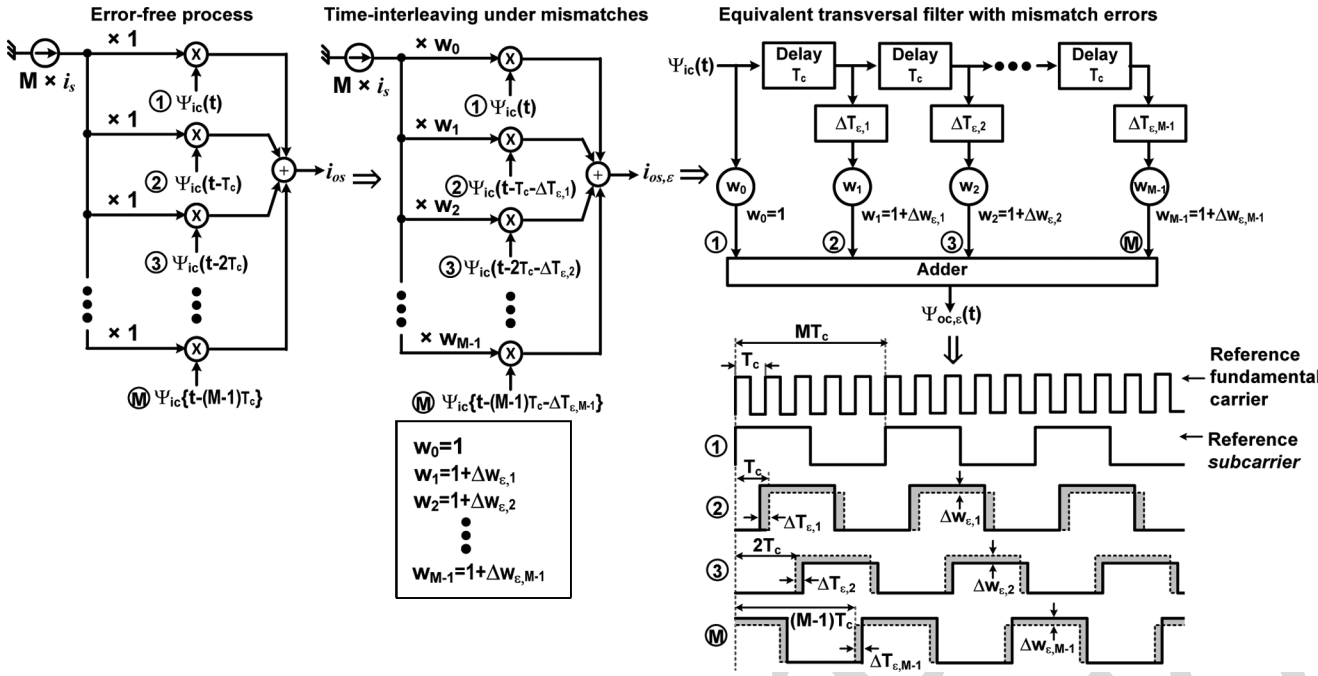

Fig. 15. Time-interleaving process with errors from gain and delay mismatches among the array elements (the dotted rectangular pulses are ideal subcarriers). $\Delta T_{\varepsilon,n}$ (n = 1 to M-1) represents delay mismatch in each subcarrier with reference to the subcarrier of ①. $\Delta w_{\varepsilon,n}$ (n = 1 to M-1) expresses gain mismatch from in each array path with reference to the path modulated by the subcarrier of ①.

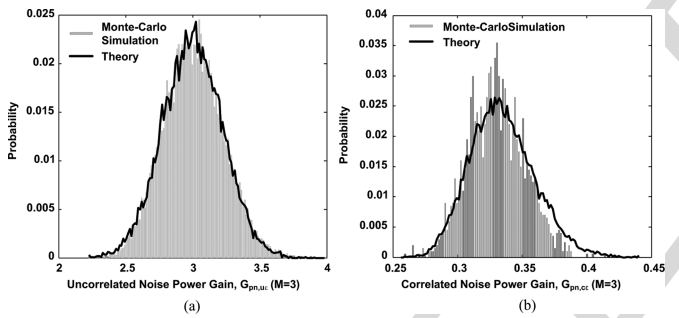

Fig. 16. Statistical mismatch simulation results of noise power gains in the TI-mixer arrays without noise filtering ($M = 3$, duty-cycle of subcarriers = 50%): (a) UNTI-mixer array, and (b) CNTI-mixer array. Bar graphs are the results from Monte-Carlo simulations in ADS. 1σ-variance of $\overline{\tau_\varepsilon} = \pm 2\%$ and 1σ-variance of T_c of (equivalently $\pm 2.4^\circ$ of 1σ phase-variance).

$$G_{pn,u\varepsilon} = \left\{1 + \left(1 + \overline{W_\varepsilon}\right)^2 (M-1)\right\} \sum_{m=-\infty}^{\infty} |\Psi_{ic}(f)|^2 \cong \left\{M + 2(M-1)\overline{W_\varepsilon}\right\} \sum_{m=-\infty}^{\infty} |\Psi_{ic}\left(\frac{m}{MT_c}\right)|^2. \quad (24)$$

It should be noted that due to a lack of coherence among the noises in the UNTI-mixer arrays, the output noise power and therefore $G_{pn,u\varepsilon}$ is not dependent of phase mismatches, but proportional to the variance of the amplitude mismatches. For the CNTI-mixer arrays in Fig. 9(b), the *correlated* noise power gain under the mismatches, $G_{pn,c\varepsilon}$ corresponding to in (19), will be approximated as (25), shown at the bottom of the page.

$$\begin{aligned} \mathrm{T}_\varepsilon(f) &= \mathrm{T}_\varepsilon\left(\frac{m}{MT_c}\right), m = integer \\ &= 1 + \sum_{\beta=1}^{M-1} \left(\underbrace{(1 + \Delta w_{\varepsilon,\beta}) e^{-j2m\pi\Delta T_{\varepsilon,\beta}/MT_c}}_{\substack{\Delta \\ complex\ weight}} \right) e^{-j2m\beta\pi/M} \\ &\cong 1 + \sum_{\beta=1}^{M-1} \left(\underbrace{\left(1 + \overline{W_\varepsilon}\right) e^{-j2m\beta\pi\overline{\tau_\varepsilon}/MT_c}}_{\substack{\Delta \\ \Delta w_{\varepsilon,\beta} \cong \overline{W_\varepsilon} \\ \Delta T_{\varepsilon,\beta} \cong \beta\overline{\tau_\varepsilon}}} \right) e^{-j2m\beta\pi/M} \\ &= 1 + \left(1 + \overline{W_\varepsilon}\right) \left(\frac{sin\left(\frac{m\pi}{M}\left(1 + \frac{\overline{\tau_\varepsilon}}{T_c}\right)(M-1)\right)}{sin\left(\frac{m\pi}{M}\left(1 + \frac{\overline{\tau_\varepsilon}}{T_c}\right)\right)} \right) e^{-jm\pi(1+\overline{\tau_\varepsilon}/T_c)} \end{aligned} \quad (21)$$

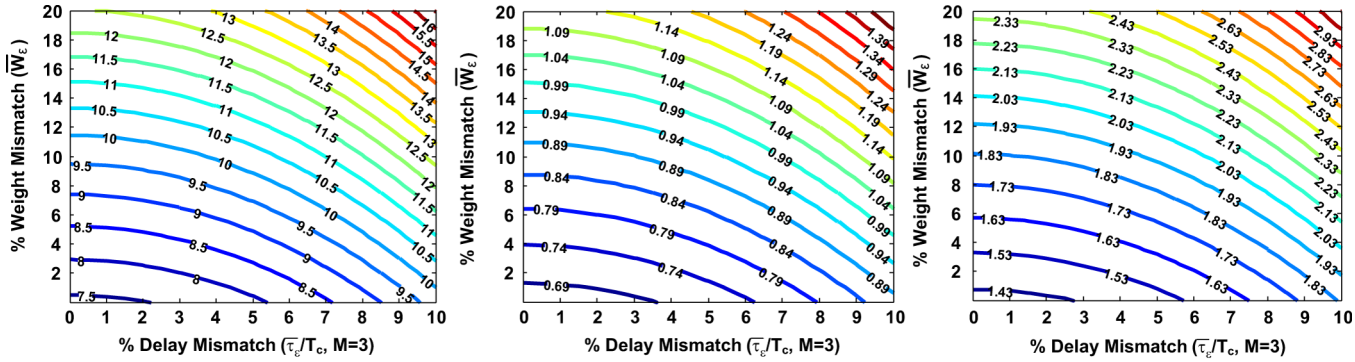

Fig. 17. Contour plots of the noise factor, $F(m=3)$ in (13), of UNTI-mixer arrays with $M=3$ (duty-cycle: 50%) under weight and delay mismatches: (a) noise factor without noise filtering, (b) noise factor with an ideal bandpass noise filtering, and (c) noise factor with an ideal high-pass noise filtering (only fundamental tone, , is rejected by an ideal HPF).

B. Mismatch Behavioral Simulations

The mismatch models have been verified through Monte-Carlo (MC) mismatch simulations in ADS. Typical simulation results are shown in Fig. 16 for the case of $M=3$. The differential subcarrier $\Psi_{s,①}(t)$ with 50% duty-cycle is utilized. It can be confirmed from the MC simulations that the worst case error distribution happens when $\Delta w_{\varepsilon,1}$ and $\Delta w_{\varepsilon,2}$ have a perfect correlation; and $\Delta T_{\varepsilon,\beta}$ ($\beta=1$ and 2) in Fig. 15 accumulates coherently across the delay chain as discussed. For a conservative estimation, the Gaussian mismatch variables have been set as following in the ADS MC simulations: two independent variables of $\Delta w_{\varepsilon,1}$ and $\Delta w_{\varepsilon,2}$ are set as the same variable with $\pm 5\%$ of 1σ–variance; and $\Delta T_{\varepsilon,2} = 2\Delta T_{\varepsilon,1}$ where $\Delta T_{\varepsilon,1}/T_c$ has $\pm 2\%$ of 1σ–variance and $\Delta T_{\varepsilon,2}/T_c$ has $\pm 4\%$ of 1σ–variance, respectively. Figs. 16(a) and 16(b) show probability distributions after 2000 ADS MC runs for each case of UNTI- and CNTI-mixer arrays, respectively. The theoretical distributions in Fig. 16 have been estimated using (24) and (25) in MATLAB statistical simulations: 1σ–variances of $\overline{W_\varepsilon}$ and $\overline{\tau_\varepsilon}/T_c$ are 5% and 2%, respectively. There is a good agreement between the ADS MC simulations and the theoretical estimations.

For the UNTI-array ($M=3$) under the weight and delay mismatches, noise factor $F(m=3)$ has been calculated based on (23) and (24). Fig. 17 displays contour plots of the noise factors which are well agreed with ADS behavioral simulation results. Fig. 17(a) show the noise factor without noise filtering. Figs. 17(b) and 17(c) are the cases with an ideal bandpass and highpass noise filtering, respectively. As expected, the TI-mixer array with *uncorrelated* noises exhibits a high sensitivity to the mismatches (reference: when and without noise filtering, F(3)$= 3/0.405 = 7.4$). The bandpass and highpass noise filtering, however, reduce the sensitivity to the mismatches dramatically in the UNTI-mixer array. From ADS MC simulations, it can also be confirmed that in CNTI-mixer arrays sensitivity to mismatches can be reduced substantially by a bandpass noise filtering as well.

VI. Conclusions

This paper proposes a time-interleaved carrier modulation and demodulating technique. The present method is essentially a mixer array technique relying on a parallel interleaving of a series of modulated outputs in the time domain. The time-interleaved mixer array inherits a filtering function from a transversal filter, and the time interleaving process is equivalent to a selective filtering of a fundamental tone and its harmonics of carrier signals. A carrier waveform and duty-cycle play a critical role in the noise performance of the arrays, and a comprehensive noise analysis is presented for both correlated and uncorrelated noises. Analytical mismatch models are provided and verified through ADS Monte-Carlo simulations. The time-interleaved array technique will allow a high-speed in carrier modulations and demodulations with a trade off a system complexity. It will be a promising solution to realize high-frequency frequency mixing systems extending over millimeter and sub-millimeter wave regime under a limitation of active device speed.

$$\begin{aligned}\overline{i_{on,c\varepsilon}(f)} &= \frac{\overline{i_n(f)}}{\sqrt{M}} \circledast \Psi_{ic}(f) \circledast \mathrm{T}_\varepsilon(f) \\ &= \frac{\overline{i_n^2}}{M} |\Psi_{ic}(f)\,\mathrm{T}_\varepsilon(f)|^2 \\ G_{pn,c\varepsilon} &\cong \sum_{m=-\infty}^{\infty} \left(\frac{\frac{1}{M} \times \left|\Psi_{ic}\left(\frac{m}{MT_c}\right)\right|^2 \times}{\left(1+\left(1+\overline{W_\varepsilon}\right)\cos m\pi \left(\frac{\sin\left(\frac{m\pi}{M}\left(1+\frac{\overline{\tau_\varepsilon}}{T_c}\right)(M-1)\right)}{\sin\left(\frac{m\pi}{M}\left(1+\frac{\overline{\tau_\varepsilon}}{T_c}\right)\right)}\right)\right)^2} \right) \end{aligned} \quad (25)$$

REFERENCES

[1] "IEEE standard 802.15.3c, wireless medium access control (MAC) and physical layer (PHY) specifications for high rate wireless personal area network (WPANs)," *Amendment 2: Millimeter-Wave Based Alternative Physical Layer Extension, Ratified 12*, Oct. 2009.

[2] A. Hirata, T. Kosugi, H. Takahashi, J. Takeuchi, H. Togo, M. Yaita, N. Kukutsu, K. Aihara, K. Murata, Y. Sato, T. Nagatsuma, and Y. Kado, "120-GHz-Band wireless link technologies for outdoor 10-Gbit/s data transmission," *IEEE Trans. Microw. Theory Tech.*, vol. 60, no. 3, pp. 881–895, Mar. 2012.

[3] J. Federici and L. Moeller, "Review of terahertz and subterahertz wireless communications," *J. Appl. Phys.*, vol. 107, no. 11, p. 111101, Jun. 2010.

[4] S. K. Reynolds, "A 60-GHz superheterodyne downconversion mixer in silicon-germanium bipolar technology," *IEEE J. Solid-State Circuits*, vol. 39, no. 11, pp. 2065–2068, Nov. 2004.

[5] A. Parsa and B. Razavi, "A new transceiver architecture for the 60-GHz band," *IEEE J. Solid-State Circuits*, vol. 44, no. 3, pp. 751–762, Mar. 2009.

[6] F. Vecchi, S. Bozzola, M. Pozzoni, D. Guermandi, E. Temporiti, M. Repossi, U. Decanis, and A. Mazzanti, "A wideband mm-Wave CMOS receiver for Gb/s communications employing interstage coupled resonators," *Proc. ISSCC Dig. Tech. Papers*, pp. 220–221, Feb. 2010.

[7] B. R. Jackson and C. E. Saavedra, "A CMOS ku-band 4x subharmonic mixer," *IEEE J. Solid-State Circuits*, vol. 43, no. 6, pp. 1351–1359, Jun. 2008.

[8] H. Takahashi, T. Kosugi, A. Hirata, K. Murata, and N. Kukutsu, "10-Gbit/s quadrature phase-shift-keying modulator and demodulator for 120-GHz-Band wireless links," *IEEE Trans. Microw. Theory Tech.*, vol. 58, no. 12, pp. 4072–4078, Dec. 2010.

[9] J.-D. Park, S. Kang, and A. M. Niknejad, "A 0.38 THZ fully integrated transceiver utilizing a quadrature push-push harmonic circuitry in sige bicmos," *IEEE J. Solid-State Circuits*, vol. 47, no. 10, pp. 2344–2354, Oct. 2012.

[10] K. W. Kobayashi, A. K. Oki, L. T. Tran, J. C. Cowles, G. Gutierrez-Aitken, F. Yamada, T. R. Block, and D. C. Streit, "A 108-GHz InP-HBT monolithic push-push VCO with low phase noise and wide tuning bandwidth," *IEEE J. Solid-State Circuits*, vol. 34, no. 9, pp. 1225–1232, Sep. 1999.

[11] K. K. O, M. C. F. Chang, M. Shur, and W. Knap, "Sub-millimeter wave signal generation and detection in CMOS," in *Proc. MTT-S Int. Microw. Symp. Dig.,–188*, Jun. 2009, p. 185.

[12] E. Seok, D. Shim, C. Mao, R. Han, S. Sankaran, C. Cao, W. Knap, and K. K. O, "Progress and challenges towards terahertz CMOS integrated circuits," *IEEE J. Solid-State Circuits*, vol. 45, no. 8, pp. 1554–1563, Aug. 2010.

[13] W. C. Black and D. A. Hodges, "Time interleaved converter arrays," *IEEE J. Solid-State Circuits*, vol. SC-15, no. 12, pp. 1022–1029, Dec. 1980.

[14] C. S. G. Conroy, D. W. Cline, and P. R. Gray, "An 8-b 85-MS/s parallel pipeline A/D converter in 1-mm CMOS," *IEEE J. Solid-State Circuits*, vol. 28, 4, no. 4, pp. 447–454, Apr. 1993.

[15] D. Camarero, K. B. Kalaia, J.-F. Naviner, and P. Loumeau, "Mixed-signal clock-skew calibration technique for time-interleaved adcs," *IEEE Trans. Circuits Syst. I, Reg. Papers*, vol. 55, no. 11, pp. 3676–3687, Dec. 2008.

[16] A. V. Oppenheim, R. W. w. Schafer, and J. R. Buck*, Discrete-Time Signal Processing*, 2nd ed ed. Upper Saddle River, NJ, USA: Prentice Hall, 1999.

[17] *Advanced Design System (ADS)*. Santa Clara, CA, USA: Agilent Technology Inc..

[18] L. W. Couch*, Digital and Analog Communication Systems*, 6 ed. Upper Saddle River, NJ, USA: Prentice Hall, 2000.

[19] K.-J. Koh, M.-Y. Park, C.-S. Kim, and H.-K. Yu, "Subharmonically pumped CMOS frequency conversion (up and down) circuits for 2-GHz WCDMA direct-conversion transceiver," *IEEE J. Solid-State Circuits*, vol. 39, no. 6, pp. 871–884, Jun. 2004.

[20] H.-C. Chen, T. Wang, H.-W. Chiu, Y.-C. Yang, T.-H. Kao, G.-W. Huang, and S.-S. Lu, "A 5-GHz-band CMOS receiver with low LO self-mixing front end," *IEEE Trans. Circuits Syst. I, Reg. Papers*, vol. 56, no. 4, pp. 705–713, Apr. 2009.

[21] S. He and C. E. Saavedra, "An Ultra-Low-Voltage and Low-Power $\times 2$ Subharmonic Downconverter Mixer," *IEEE Trans. Microw. Theory Tech.*, vol. 60, no. 2, pp. 311–317, Feb. 2012.

[22] R. V. Gatti, M. Dionigi, and R. Sorrentino, "Computation of gain, noise figure, and third-order intercept of active array antenna," *IEEE Trans. Antennas Propagat.*, vol. 52, no. 11, pp. 3139–3142, Nov. 2004.

[23] P. Z. Peebles*, Probability, Random Variables, and Random Signal Principles*, 3 ed. New York, NY, USA: McGraw-Hill, 1993.

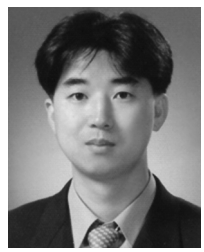

Kwang-Jin Koh (S'06–M'09) received the B.S. degree in electronic engineering (first-class honors) from Chung-Ang University, Seoul, Korea, in 1999, the M.S. degree in electrical engineering from the Korea Advanced Institute of Science and Technology (KAIST), Daejeon, Korea, in 2001, and the Ph.D. degree in electrical and computer engineering from the University of California at San Diego, La Jolla, CA, USA, in 2008.

In November 2011, he joined the Electrical and Computer Engineering Department, Virginia Polytechnic Institute and State University (Virginia Tech), Blacksburg, as an Assistant Professor. From 2001 to 2004, he was with the Electronics and Telecommunications Research Institute (ETRI), Daejeon, Korea, where he was engaged in the research and development of RF and analog CMOS integrated circuits for wireless communication systems. From 2008 to 2010, he was with the Portland Technology Group (PTD), Intel Corporation, as a Senior Engineer, where he was involved in the development of voltage-controlled oscillators (VCOs) and phase-locked loops (PLLs) in Intel 32- and 22-nm CMOS processes for Intel microprocessors and radios applications. From 2010 to 2011, he was with the Broadcom Corporation, as a Senior Staff Scientist, where he developed RF integrated circuits (RFICs) for digital TV tuner systems-on-a-chip. His research interests include analog, RF and millimeter-wave integrated circuits and systems wireless communications, radars, and imaging applications.

Dr. Koh was the recipient of the 2002 Best Paper Award of the IEEE Solid-State Circuits Society and Electron Device Society, Seoul Chapter. His Ph.D. works on integrated phased arrays on silicon technologies have been reported to the U.S. Pentagon as part of a Defense Advanced Research Projects Agency (DARPA) War Report as one of the major accomplishments of 2007. He was also the recipient of the 2010 Best Team of the Year Award of the Teledyne Scientific Corporation (formerly the Rockwell Scientific Corporation), and 2012 Virginia Tech ICTAS Junior Faculty Research Award.

Seyed Yahya Mortazavi (S'07) received the B.S. degree in electrical engineering from University of Tehran, Tehran, Iran, in 2003 and the M.S. degree in electrical engineering from Tarbiat-Modares University, Tehran, Iran, in 2005. The M.S. research was on high-speed folding-Interpolating ADC design, and continued on wide-bandwidth high-resolution sigma-delta ADCs until 2010. He is currently working toward the Ph.D. degree in electrical engineering at Virginia Tech (VT), Blacksburg, VA, USA.

His research interests include system and circuit design for RF and mm-Wave integrated communication transceivers, and Imaging systems.

Sadia Afroz (S'10) received the B.S. degree in electrical engineering from Bangladesh University of Engineering and Technology, Bangladesh, in 2011. She is currently working toward the Ph.D. degree at Virginia Tech, Blacksburg, VA, USA.

Her research was on high-speed Ultra wideband Inter and intra-chip wireless communication system until 2011. Her current research interests include design of millimeter-wave circuits, wireless transceiver and Phased-array architectures.

Time Interleaved RF Carrier Modulations and Demodulations

Kwang-Jin Koh, *Member, IEEE*, Seyed Yahya Mortazavi, *Student Member, IEEE*, and Sadia Afroz, *Student Member, IEEE*

***Abstract*—This paper proposes a time-interleaved RF carrier modulation and demodulation technique, suitable for high frequency mixer applications under a constraint of active device speed limitation. The presents are in essence mixer arrays where modulated outputs by a series of time-delayed carriers with a reduced frequency, compared with a carrier frequency in fundamental mixers, will be interleaved in the time domain to synthesize the final output. The mixer arrays inherit an FIR filtering function, and the time interleaving process is equivalent to the filtering process where the arrays select the fundamental tone or its harmonics of a carrier in a periodic manner. The carrier waveform and duty-cycle play important roles in the noise performance of the mixer arrays. A comprehensive noise analysis is presented in this paper for both cases of correlated-noise and uncorrelated-noise mixer arrays. To minimize output noise power, optimization of carrier duty-cycle and noise filtering technique have been proposed and analyzed extensively for various types of carrier pulse. Finally analytical mismatch models are provided and output SNR degradations under finite mismatches amongst mixer array elements have been discussed based on the mismatch models. All theoretical analyses are verified through behavioral mixer array simulations including Monte-Carlo statistical simulations.**

***Index Terms*—Array, demodulator, FIR filter, mixer, mixer array, modulator, multiphase, radio frequency, time interleaving, transversal filter, wireless communications.**

I. Introduction

RECENTLY wireless communications at millimeter (mm)-wave and submillimeter wave ranges have been gaining growing attentions to achieve a high data-rate over several 10's Gb/s [1]–[3]. One of key technical huddles in realizing the high-speed communications in integrated circuit technologies is the carrier modulations and demodulations, due to a lack of carrier source having a high spectral purity with an adequate output power at such high frequencies. To circumvent the issue from the system perspective, heterodyne architectures have been adopted to reduce required carrier frequency at the expense of a hardware complexity and image issue involved in the double conversions [4]–[6]. A subharmonic mixing (e.g., 2x, 4x even-harmonic carrier modulation) has been another popular choice for a minimum amount of signal processing at the mm-waves and therefore to relieve the speed burden on the local oscillator (LO) paths in the mm-wave mixer designs [7]–[9]. A constant progress has also been made to push oscillation frequency of voltage controlled oscillators over sub-terahertz realms in solid-state electronics [10]–[12]. Yet because of a limited active device speed, major challenges have been posed in implementing practical carrier modulation and demodulation systems with a fundamental mixer at the high-end of the mm-wave regimes [12].

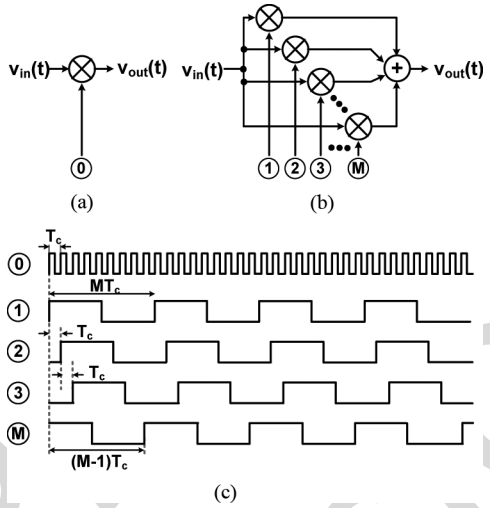

Fig. 1. (a) Fundamental mixer (modulation frequency: $f_c = 1/T_c$), (b) time-interleaved (TI) mixer array with a time-interleaving factor of M (modulation frequency: f_c/M), and (c) rectangular pulse trains for the fundamental mixer and the TI mixer arrays.

In this paper, a time-interleaved carrier modulation and demodulation technique has been proposed to enable mm-wave and submillimeter wave frequency mixers under the constraints of the device speed limitations. Fig. 1(b) illustrates a time-interleaved carrier modulator which is essentially a mixer array where each mixer modulates the input signal with a reduced frequency, compared with the fundamental mixer in Fig. 1(a). By interleaving the modulated outputs from individual mixers, the final output will contain the same frequency information as in the fundamental mixer. An essential benefit in the time-interleaved modulation is that the carrier frequency can be reduced by a factor of the number of time interleaving. This allows less speed burden on electronics generating carrier signals, which will be a particular benefit when realizing high-speed communication electronics in silicon processes suffering from a relatively low device speed compared with that of compound semiconductors [13]–[15].

The time-interleaved mixer arrays inherit a filtering function of a transversal filter [16], and the interleaving process is essentially a filtering process where fundamental tone and its harmonics of a carrier can be filtered selectively, which is elaborated in Section II. The waveform and duty-cycle of carriers

Manuscript received February 12, 2013; revised May 17, 2013; accepted June 24, 2013. This paper was recommended by Associate Editor J. Ma.

The authors are with the Department of Electrical and Computer Engineering, Virginia Tech, Blacksburg, VA 24061 USA (e-mail: kkoh@vt.edu).

Color versions of one or more of the figures in this paper are available online at http://ieeexplore.ieee.org.

Digital Object Identifier 10.1109/TCSI.2013.2278387

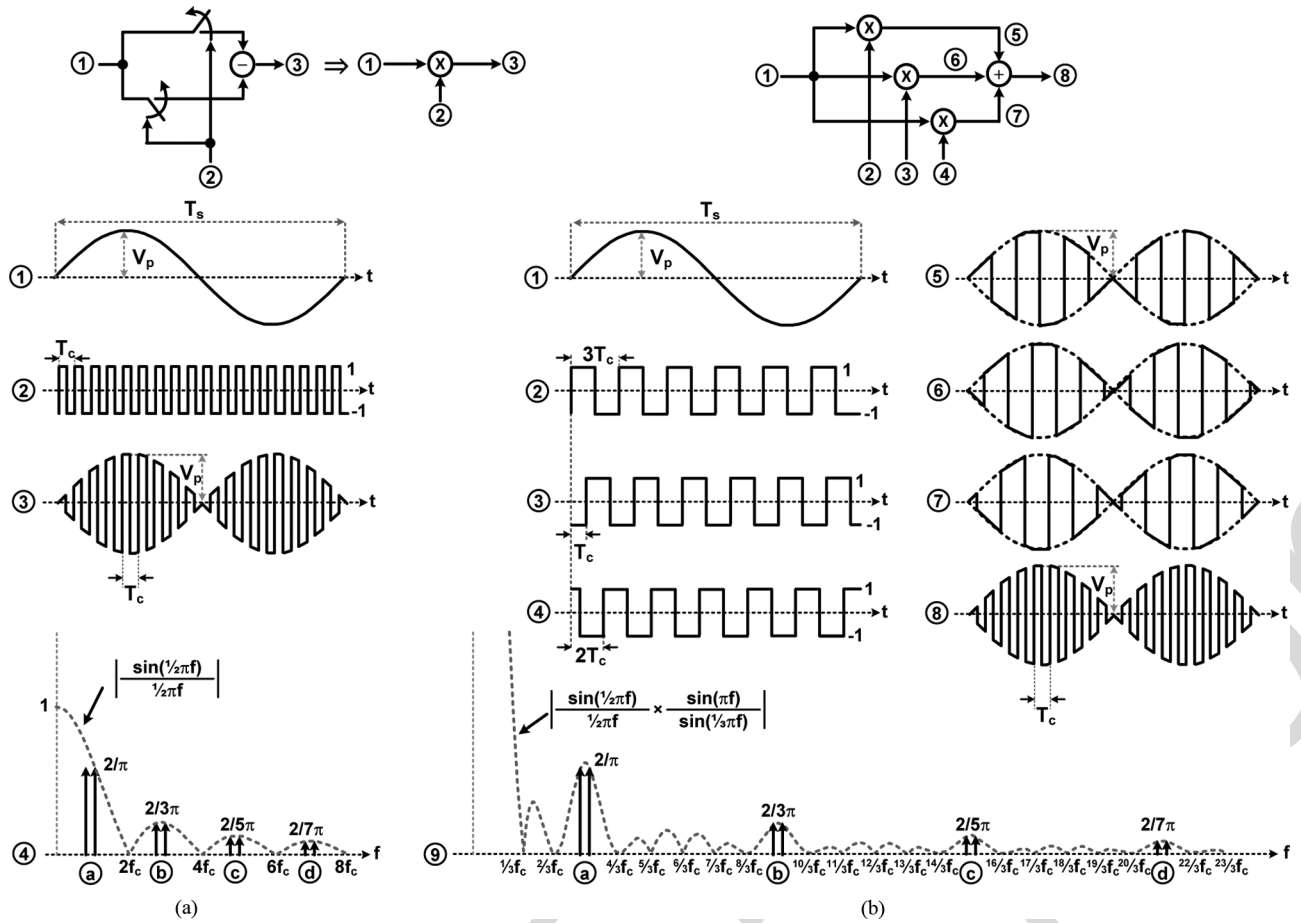

Fig. 2. Fundamental and time-interleaved carrier modulations with bipolar differential carriers: (a) modulation with fundamental carrier frequency using bipolar *on-off* switches (① :input signal; ② : bipolar rectangular carrier pulse; ③ : modulated output; and ④ : spectral components of the output normalized by the input peak magnitude), (b) time-interleaved modulation with $1/3f_c$ of carrier frequency (time interleaving factor: 3, ① : input signal; ②, ③ and ④ : bipolar rectangular *subcarrier* pulses; ⑤, ⑥ and ⑦ : modulated outputs by ②, ③ and ④, respectively; ⑧ : final time-interleaved output; and ⑨ : spectral components of the output normalized by the input peak magnitude). For both cases, ⓐ $= f_c \pm f_s$, ⓑ $= 3f - c \pm f_s$, ⓒ $= 5f - c \pm f_s$, and ⓓ $= 7f - c \pm f_s$.

play important roles in the noise performance of the arrays. An extensive noise analysis is presented in Sections III and IV. Optimization of the duty-cycle and noise filtering technique to relieve the noise issue are proposed in Section IV. The mixer array will be subjected to mismatches between array elements and analytical mismatch models have been provided in Section V. All the theories in the paper have been verified through behavioral mixer simulations including Monte-Carlo statistical simulations in Advance Design System (ADS) [17].

II. Time Interleaved Carrier Modulations

Carrier modulation is fundamentally a multiplication process and Fig. 2(a) shows a typical way of realizing the carrier multiplication relying on the *on-off* switch modulation [18]. The bipolar differential square-wave having 50% duty-cycle, expressed as (1) in the frequency domain, turns *on* each switch differentially per cycle. This will modulate input signal $v_s(t) = V_p sin(2\pi f_s t)$ where $f_s = 1/T_s$. By adding each switch output differentially the final modulated output is illustrated as ③ in the time domain.

$$\Psi_{bc}(f) = \sum_{m=1}^{\infty} \frac{4}{\pi} \frac{sin\left(\frac{m\pi}{2}\right)}{m} e^{-jm\pi/2} \delta(f - mf_c). \quad (1)$$

Equivalently, the input signal will be convoluted by $\Psi_{bc}(f)$ in the frequency domain, resulting in a series of frequency modulation of the input by the fundamental tone and its harmonics of $\Psi_{bc}(f)$. In Fig. 2(a) ④ shows first a few major spectral tones of the modulated output, which are normalized by the peak magnitude of the input: ⓐ $= f_c \pm f_s$, ⓑ $= 3f_c \pm f_s$, ⓒ $= 5f_c \pm f_s$, and ⓓ $= 7f_c \pm f_s$. In typical fundamental mixers, a narrowband filtering will be applied to the output in order to select the fundamentally modulated components shown as ⓐ.

Fig. 2(b) illustrates a time-interleaved (TI) modulation with a time interleaving factor of 3 to realize the same modulation functionality as in Fig. 2(a). In essence the system is a switch array and each switch will be driven by a series of the bipolar square-waves with 50% duty-cycle, called *subcarriers* represented as ②, ③ and ④, respectively. The subcarrier frequency will be reduced by the time-interleaving factor, compared with the fundamental mixer. From the reference of the subcarrier ②, the subcarriers ③ and ④ undergo a successive cumulative delay of T_c. Modulations of input signal by each subcarrier ②, ③ and ④ will output ⑤, ⑥ and ⑦, respectively. An instantaneous combining (or interleaving) of all the outputs gives the final output of ⑧ which contains the same spectral components as in Fig. 2(a).

In general the reference subcarrier ② can be expressed in terms of the fundamental carrier frequency of f_c. This is given

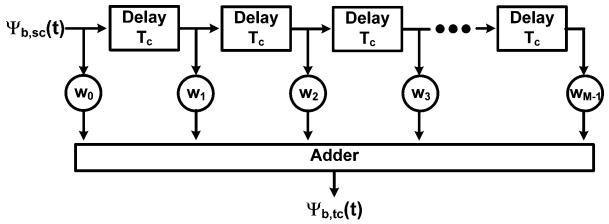

Fig. 3. A transversal filter equivalent to the delay-sum operation in the time-interleaved carrier signal in (3): $\mathrm{w}_0 = \mathrm{w}_1 = \mathrm{w}_2 = \mathrm{w}_3 = \mathrm{w}_{M-1} = 1$.

as (2) in the frequency domain for an arbitrary *odd* number of the time-interleaving factor M.

$$\Psi_{b,sc}(f) = \sum_{m=-\infty}^{\infty} \frac{4}{\pi} \frac{sin\left(\frac{m\pi}{2}\right)}{m} e^{-jm\pi/2} \delta\left(f - \frac{m}{M} f_c\right), \quad M = odd. \tag{2}$$

Consequently, the summation of total subcarriers will be

$$\begin{aligned}\Psi_{b,tc}(f) &= \sum_{k=0}^{M-1} \Psi_{b,sc}(f)\, e^{-jk2\pi f T_c}, M = odd \\ &= \Psi_{b,sc}(f) \frac{\sin(M\pi f T_c)}{\sin(\pi f T_c)} e^{-j(M-1)\pi f T_c}, f = \frac{m f_c}{M} \\ &= \Psi_{b,sc}(f) \frac{\sin(m\pi)}{\sin\left(\frac{m\pi}{M}\right)} e^{-jm(M-1)\pi/M}, m = M \times odd \\ &= \sum_{n=1}^{\infty} \frac{4}{\pi} \frac{\sin\left(\frac{Mn\pi}{2}\right)}{n} e^{-jMn\pi/2} \delta(f - n f_c). \end{aligned} \tag{3}$$

In (3), $2\pi f T_c$ is a phase delay caused by the time delay of T_c for the subcarriers having $\mathrm{f_c/M}$ of frequency. Thanks to the sinusoidal periodicity, it can be shown that $\Psi_{b,tc}(f) = \Psi_{bc}(f)$, and the TI-modulation is a convolution of the input with the $\Psi_{b,tc}(f)$. In the frequency domain, the final modulated output after the interleaving process will be

$$v_{out}(f) = \Psi_{b,tc}(f) \circledast v_s(f) = \Psi_{bc} \circledast v_s(f). \tag{4}$$

Note that under the constraint of 50% duty-cycle in the subcarriers only *odd* number of time interleaving is allowed. The limitation is due to the fact that the time interleaving process is inherently a filtering process: i.e., the term $\sum_{k=0}^{M-1} e^{-jk2\pi f T_c}$ in (3) represents a transfer function from the transversal filter where filter taps have unity weight after a successive time delay of T_c[16]. The transversal filter equivalence in the time domain is shown in Fig. 3 where $\mathrm{w}_0 = \mathrm{w}_1 = \mathrm{w}_2 = \mathrm{w}_3 = \mathrm{w}_{M-1} = 1$. $\Psi_{b,sc}(t)$ and $\Psi_{b,tc}(t)$ are the time domain representations of $\Psi_{b,sc}(f)$ and $\Psi_{b,tc}(f)$, respectively. The direct-form transversal filter can select (or reject) only the spectral tones comprising $\Psi_{b,sc}(t)$. With 50% duty-cycle, $\Psi_{b,sc}(f)$ in (2) contains fundamental tone of f_c/M and its odd harmonics of mf_c/M $(m = odd)$. Therefore, in order to filter the desired spectral tone of f_c, the length of the transversal filter (or the time-interleaving factor of M) needs to be an *odd* integer larger than 1.

However, if the duty-cycle of the subcarriers is not 50% and if they have a finite DC component, i.e., waveform of the subcarriers is differentially *nonsymmetrical*, then they contain both *even* and *odd* harmonics. These are the cases illustrated as ① and ② in Fig. 4. When considering an arbitrary duty-cycle of

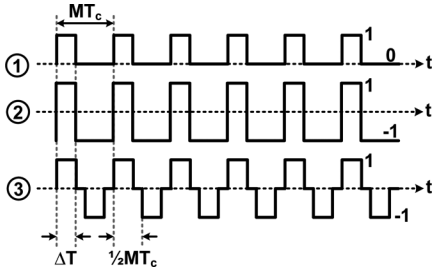

Fig. 4. Rectangular pulse subcarriers (①: a unipolar subcarrier, ②: a non-symmetrical bipolar subcarrier, and ③: an asymmetric bipolar subcarrier).

$\Delta T/(MT_c)$ for the subcarriers where MT_c is a period and ΔT is an active on-time, the waveforms of ① and ② can be expressed as (5) and (6), respectively, in the frequency domain. In these cases spectral components of the subcarriers will be $mf_c/M(m = integer)$, containing both even- and odd-order tones. Therefore, an even length M will also enable to filter the spectral tone of f_c as long as $\Delta T/(MT_c) \neq 50\%$.

$$\Psi_{\mathrm{s},1\,①}(f) = \sum_{m=-\infty}^{\infty} \frac{1}{\pi} \frac{sin\left(m\pi \frac{\Delta T}{MT_c}\right)}{m} \times e^{-jm\pi\Delta T/MT_c} \delta\left(f - \frac{m}{M} f_c\right). \tag{5}$$

$$\Psi_{\mathrm{s},\,②}(f) = \sum_{m=-\infty}^{\infty} \frac{2}{\pi} \frac{sin\left(m\pi \frac{\Delta T}{MT_c}\right)}{m} \times e^{-jm\pi\Delta T/MT_c} \delta\left(f - \frac{m}{M} f_c\right) - \delta(f). \tag{6}$$

It is worthwhile to note that the *asymmetric* (or *differentially symmetric*) bipolar subcarrier illustrated as ③ in Fig. 4, expressed as (7) in the frequency domain, contains only *odd* harmonics. Thus, only *odd* length of M is allowed to choose the f_c tone.

$$\Psi_{\mathrm{s},\,③}(f) = \sum_{m=-\infty}^{\infty} \frac{1}{\pi}(1 - cos m\pi) \frac{sin\left(m\pi \frac{\Delta T}{MT_c}\right)}{m} \times e^{-jm\pi\Delta T/MT_c} \delta\left(f - \frac{m}{M} f_c\right). \tag{7}$$

As an example, for the unipolar subcarrier in (5) the final net carrier after M times of interleaving will be given as

$$\begin{aligned}\Psi_{\mathrm{ts},\,①}(f) &= \Psi_{\mathrm{s},\,①}(f) \circledast \mathrm{T}(f) \\ &= \Psi_{\mathrm{s},\,①}(f) \circledast \sum_{\beta=0}^{M-1} e^{-j2\pi f \beta t_c} \\ &= \Psi_{\mathrm{s},\,①}(f) \frac{sin(m\pi)}{sin\left(\frac{m\pi}{M}\right)} e^{-jm(M-1)\pi/M}, \\ & m = integer, \end{aligned} \tag{8}$$

where $T(f) = \sum_{\beta=0}^{M-1} e^{-j2\pi f \beta T_c}$ is the transfer function of the transversal filter in Fig. 3. When $M = 2$, from (5) and (8) it can be found that $\Delta T/(MT_c) = 25\%$ or 75% will give the maximum 2nd -harmonic power, leading to the maximum output power when the input is modulated by the 2nd-harmonic tone. Fig. 5 illustrates the cases of $M = 2$ with 25% and 75% duty-cycles, which essentially represents a behavioral model of the 2x

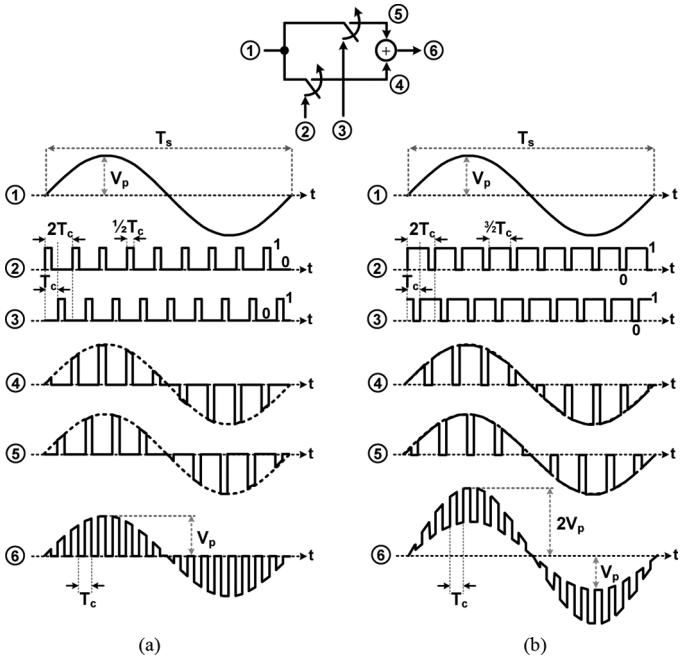

Fig. 5. Time-interleaved carrier modulation with interleaving factor $M = 2$: (a) 25% duty-cycle, (b) 75% duty-cycle.

subharmonic mixer found in many RF applications [19]–[21]. In essence, the 2x and 4x subharmonic mixers [7] can be regarded as subsets of the TI mixer array, corresponding to $M = 2$ and $M = 4$, respectively. For both cases in Fig. 5, the interleaving of ④ and ⑤, which are modulated outputs by the subcarrier ② and ③, respectively, will output the final waveforms of ⑥. The final outputs (Figs. 5(a) and 5(b)) will have the same spectral components as those in Fig. 2 except for the input leakage tone which is modulated by the DC component of the subcarriers. The magnitude of the input leakage to the output will be 3 times larger when the duty-cycle is 75%, because the average total subcarrier power (or DC power) is 3 times larger when $\Delta T/(MT_c) = 75\%$ than when $\Delta T/(MT_c) = 25\%$. The larger carrier power will produce larger output noise, which will be detailed in the next sections.

III. Noise in Carrier Demodulations

Carrier demodulation is a reciprocal process of the carrier modulation, and in general noise is of particular concern in the demodulation process since incoming signal power tends to be weak, susceptible to the system noises in typical wireless communication systems. Consider the abstraction of a single balance mixer shown in Fig. 6(a), which demodulates a modulated signal (presumably an RF signal) and translates the signal frequency, f_s, down to an intermediate frequency of $f_{IF} = f_c - f_s$ (high-side carrier injection). In a typical realization of the carrier demodulator in FET technologies, input voltage signal $(v_s = v_{s,rms} sin\omega_s t)$ will be gated to the transconductor $(\mathrm{M_c})$. The transconductor will transform the input signal into a current $(i_s = i_{s,rms} sin\omega_s t)$, while generating a noise current $(\overline{i_n})$ as well. For simplification, let's assume the noise current is white Gaussian noise, which will be a reasonable assumption for typical down-conversion mixers. In the single-balanced demodulation, the signal and noise currents will be modulated by the switch pair $(\mathrm{M_{s1,2}})$ driven by the carriers ⓐ and ⓑ, effectively turning the switch pair *on* and *off* alternatively per period. The

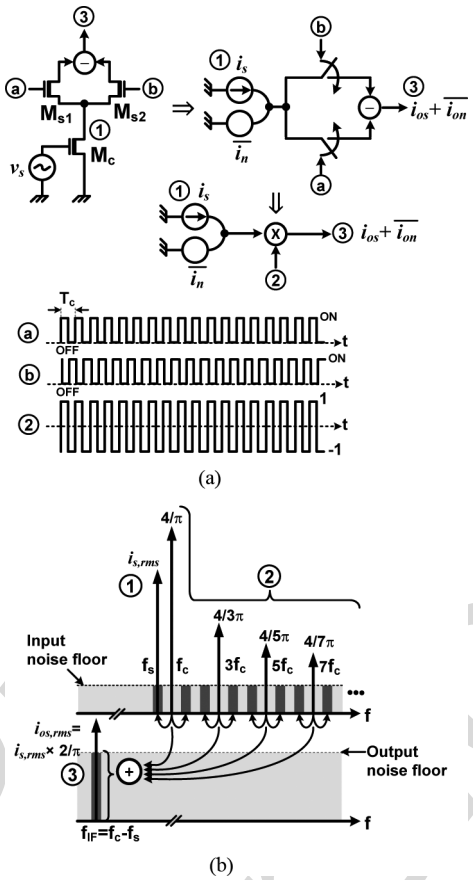

Fig. 6. (a) Single-balanced switching mixer (ⓐ and ⓑ : square-waves turning switch $\mathrm{M_{s1,2}}$ *on* and *off* alternatively, ① : transconductor output signal and noise currents, ② : bipolar square-wave equivalent to the switch *on-off* modulation, and ③ : demodulated signal and noise outputs), (b) conceptual description of the signal and noise demodulation in one-sided spectral domain (① : input signal current to the demodulator, ② : spectral tones of the bipolar square-wave, and ③ : demodulated signal and noise outputs).

demodulated signal and noise will be taken differentially at the output of ③. The demodulation process is equivalent to modulating the i_s and $\overline{i_n}$ with a unity bipolar carrier illustrated as ② and taking the intermediate output tone.

In the example, the carrier demodulation involves only a half power of the fundamental carrier tone (f_c), and the other half power will contribute to the modulation of the signal to a higher frequency of $f_c + f_s$. In Fig. 6(b) the input noise floor will be set by the transconductor noise $\overline{i_n}$. Assuming 50% duty-ratio in the bipolar pulse train, the carrier contains fundamental and its odd harmonic tones. A uniqueness in the demodulations with rectangular pulse trains is that while signal will be modulated down to a desired IF-band by a tone (usually by a fundamental tone), noise will be modulated by all harmonics as well as by the fundamental tone since the noise is essentially a thermal noise causing a frequency aliasing. This is illustrated in Fig. 6(b) where every noise spectrum distancing $+f_{IF}$ offset (upper sideband) or $-f_{IF}$ offset (lower sideband) from the fundamental tone and its harmonics will be demodulated to the same intermediate frequency as the signal, degrading the SNR at the output.

Because every spectral tone of a carrier pulse will contribute to the noise demodulation, overall power gain factor for the demodulated noise $(G_{pn} = \overline{i_{on}^2}/\overline{i_n^2})$ will be the same as the carrier power, recalling Parseval's power theorem [18]. The carrier waveform and duty-cycle play critical roles in the carrier

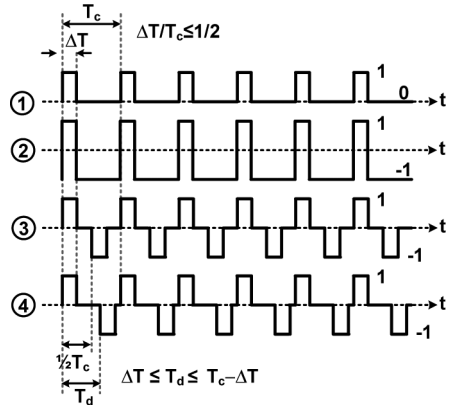

Fig. 7. Rectangular carrier pulses with a duty cycle $\Delta \mathrm{T}/\mathrm{T}_c \leq 50\%$($\mathrm{T}_c$: period, ①: $\Psi_{①}(t)$- unipolar pulse, ②: $\Psi_{②}(t)$- nonsymmetrical bipolar pulse, ③: $\Psi_{③}(t)$—asymmetric bipolar differential ($\mathrm{T}_d = 1/2\mathrm{T}_c$) pulse, and ④:$\Psi_{④}(t)$—asymmetric bipolar pulse with an arbitrary T_d under a constraint of $\Delta \mathrm{T} \leq \mathrm{T}_d \leq \mathrm{T}_c - \Delta \mathrm{T}$.

power and therefore in the output SNR. Fig. 7 shows several cases of rectangular carrier pulses with a finite duty-cycle. In the frequency domain each carrier pulse train can be expressed as (9)–(12) at the bottom of the page.

As a practical consideration the duty-cycle is limited to 50%: i.e., $\Delta T/T_c \leq 1/2$. The waveform of ③, $\Psi_{③}(t)$, is a general case of a differential pulse train having a half-period delay in the negative pulse. For a completeness of consideration, the waveform of ④, $\Psi_{④}(t)$, is included and has an arbitrary delay T_d subjected to $\Delta T \leq T_d \leq T_c - \Delta T$ for the negative pulse. $\Psi_{③}(t)$ contains only fundamental tone and its odd harmonics, but introducing T_d $(\neq T_c/2)$ in $\Psi_{④}(t)$ allows even harmonic tones in (12): note $|T_d - T_c/2| \times 2\pi f_c$ represents a differential phase mismatch which induces even harmonics in the *asymmetric* bipolar pulse train. In (12) harmonic power of the m-th tone will be maximized when $T_d/T_c = k/(2m)$ where $k = odd$ and $k/m \leq 1$.

Generally speaking, any harmonic spectral component as well as a fundamental tone in rectangular pulses can be utilized for carrier modulations and demodulations. Table I lists signal power gains ($G_{ps,m} = i^2_{os,rms}/i^2_{s,rms}$) and noise power gains ($G_{pn} = \overline{i^2_{on}}/\overline{i^2_n}$) when they are demodulated by the m-th harmonic tone of each carrier pulse in Fig. 7. The G_{pn} in the table is essentially the carrier power of each carrier type. It should be emphasized that the ratio of $G_{pn}/G_{ps,m}$ addresses a noise factor (NF) [18] of the *demodulation process itself*:

$$\begin{aligned}\text{Noise Factor} : \mathrm{F}(m) &= \frac{(SNR)_{input}}{(SNR)_{output}} \\ &= \frac{G_{pn}}{G_{ps,m}}, \end{aligned} \tag{13}$$

$$\begin{aligned}\text{Noise Figure} : \mathrm{NF}(m) &= 10 \times log \mathrm{F}(m) \\ &= 10 \times log\left(\frac{G_{pn}}{G_{ps,m}}\right). \end{aligned} \tag{14}$$

Note that NF is a function of the order of the modulation tone (m) and the carrier duty-cycle. When a carrier demodulation is conducted by a fundamental tone of the unipolar carrier of $\Psi_{①}(t)$ in Fig. 7, then $\Delta T/T_c = 25\%$ and 75% will give the same signal power gain of $G_{ps,1} = 1/(2\pi^2)$, but noise power will be different for each case: $G_{pn} = 1/4$ for $\Delta T/T_c = 25\%$ and $G_{pn} = 3/4$ for $\Delta T/T_c = 75\%$. This results in 3 times larger noise factor in the case with 75% of duty-cycle than the other case: i.e., $\mathrm{F}(1) = \pi^2/2$ for $\Delta T/T_c = 25\%$, and $\mathrm{F}(1) = 3\pi^2/2$ for $\Delta T/T_c = 75\%$. Usually a larger duty-cycle than 50% will worse noise effect and in typical designs the duty-cycle will be limited to 50% to minimize the noise degradation. This is the

---

$$\begin{aligned}&① : Unipolar \text{ carrier}, \Psi_{①}(f) \\ &= \sum_{m=-\infty}^{\infty} \frac{1}{\pi} \frac{sin\left(m\pi \frac{\Delta T}{T_c}\right)}{m} e^{-jm\pi\Delta T/T_c} \delta(f - mf_c) \end{aligned} \tag{9}$$

$$\begin{aligned}&② : Nonsymmetrical \text{ bipolar carrier}, \Psi_{②}(f) \\ &= \sum_{m=-\infty}^{\infty} \frac{2}{\pi} \frac{sin\left(m\pi \frac{\Delta T}{T_c}\right)}{m} e^{-jm\pi\Delta T/T_c} \delta(f - mf_c) - \delta(f) \end{aligned} \tag{10}$$

$$\begin{aligned}&③ : Asymmetric\ differential \text{ bipolar carrier}, \Psi_{③}(f) \\ &= \sum_{m=-\infty}^{\infty} \frac{1}{\pi} \frac{sin\left(m\pi \frac{\Delta T}{T_c}\right)}{m} (1 - cosm\pi) e^{-jm\pi\Delta T/T_c} \delta(f - mf_c) \end{aligned} \tag{11}$$

$$\begin{aligned}&④ : Asymmetric \text{ bipolar carrier with a delay} \mathrm{T}_d, \Psi_{④}(f) \\ &= \sum_{m=-\infty}^{\infty} \frac{1}{\pi} \frac{sin\left(m\pi \frac{\Delta T}{T_c}\right)}{m} \left(1 - e^{-j2m\pi T_d/T_c}\right) e^{-jm\pi\Delta T/T_c} \delta(f - mf_c), \\ &where\ \Delta T \leq T_d \leq T_c - \Delta T. \end{aligned} \tag{12}$$

TABLE I
SIGNAL POWER GAIN ($G_{\mathrm{ps,m}}$) AND NOISE POWER GAIN (G_{pn}) IN THE DEMODULATION PROCESS BY EACH CARRIER IN FIG. 7.

	$\mathbf{G_{ps,m}}$	$\mathbf{G_{pn}}$
①	$\left\{\frac{1}{m\pi}\sin\left(m\pi\frac{\Delta\mathrm{T}}{\mathrm{T}_c}\right)\right\}^2$	$\frac{\Delta\mathrm{T}}{\mathrm{T}_c}$
②	$\left\{\frac{2}{m\pi}\sin\left(m\pi\frac{\Delta\mathrm{T}}{\mathrm{T}_c}\right)\right\}^2$	1
③	$\left\{\frac{1}{m\pi}\sin\left(m\pi\frac{\Delta\mathrm{T}}{\mathrm{T}_c}\right)\right\}^2 \times(1-\cos m\pi)$	$2\frac{\Delta\mathrm{T}}{\mathrm{T}_c}$
④	$\left\{\frac{\frac{1}{m\pi}\sin\left(m\pi\frac{\Delta\mathrm{T}}{\mathrm{T}_c}\right)}{\times\sqrt{2-2\cos\left(2m\pi\frac{\mathrm{T}_d}{\mathrm{T}_c}\right)}}\right\}^2$	$2\frac{\Delta\mathrm{T}}{\mathrm{T}_c}$

Note: ①, ②, ③, and ④ represent each subcarrier type depicted in Fig. 7, respectively.

main reason for imposing the limitation of $\Delta T/T_c \leq 1/2$ as a practical consideration in this paper.

To verify the theory, behavioral mixer simulations are performed in ADS. Fig. 8 shows results when the fundamental tone ($m = 1$ in the Table I) is utilized for the carrier demodulation. The theoretical NF calculations are based on (14) by applying $G_{ps,m}$ and G_{pn} in Table I, and agreed well with the behavioral simulations. From the Table I, the optimum duty-cycle for maximum signal power gain for all cases can be given as $\Delta T/T_c = k/(2m)$ where $k = odd$ and $k \leq m$: for example, if a fundamental tone ($m = 1$) is utilized for the demodulation, then 50% duty-cycle will give the maximum signal power gain. However, the optimum duty-cycle for maximum SNR is not necessarily coincided with that for the maximum signal power gain. The output SNR will be proportional to $1/\mathrm{F}(m) = G_{ps,m}/G_{pn}$. Therefore, it is apparent from the Table I that, except for the case ②, the optimum duty-cycle minimizing the noise factor can be found as the maximizing (15), resulting in (16) as the condition for the optimum duty-cycle.

$$f\left(\frac{\Delta T}{T_c}\right) = \left\{sin\left(m\pi\frac{\Delta T}{T_c}\right)\right\}^2\left(\frac{\Delta T}{T_c}\right)^{-1},\ where\ \frac{\Delta T}{T_c} \leq \frac{1}{2} \tag{15}$$

$$\begin{aligned} & df\frac{\left(\frac{\Delta T}{T_c}\right)}{d}\left(\frac{\Delta T}{T_c}\right) = 0 \\ & \Rightarrow tan\left(m\pi\left(\frac{\Delta T}{T_c}\right)_{opt}\right)\left(m\pi\left(\frac{\Delta T}{T_c}\right)_{opt}\right)^{-1} = 2 \\ & \Rightarrow m\left(\frac{\Delta T}{T_c}\right)_{opt} \cong 0.371. \end{aligned} \tag{16}$$

When $m = 1$, $(\Delta T/T_c)_{opt}$ is about 37.1% which can be confirmed from the behavioral simulation results shown in Figs. 8(a) and 8(c). In general if the m-th harmonic tone of the carrier $\Psi_{①}(t)$ or $\Psi_{③}(t)$ in Fig. 7 is used for a carrier demodulation then the optimum duty-cycle for the maximum SNR will be $(\Delta T/T_c)_{opt} \cong 0.371/m$. For the case of $\Psi_{④}(t)$, noise power is always unity. Therefore, the duty-cycle for the maximum signal power will give the maximum SNR. It is

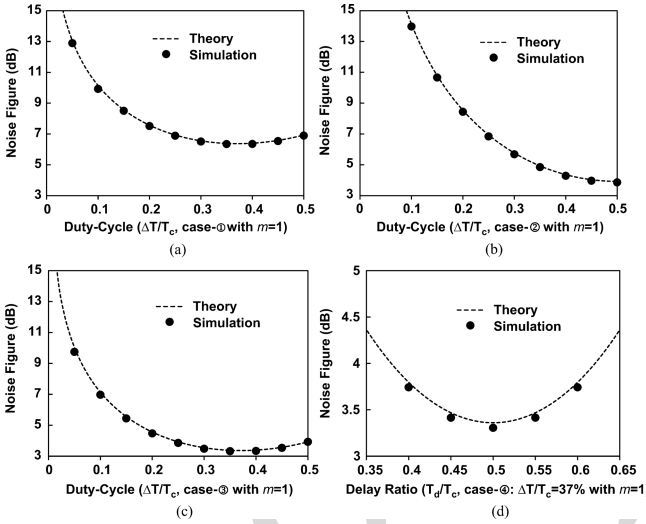

Fig. 8. Noise figure $\mathrm{NF}(m = 1)$ when the fundamental tone of each carrier in Fig. 7 is utilized for the carrier demodulation: (a) $\mathrm{NF}(m = 1)$ with the carrier $\Psi_{①}(t)$, (b) $\mathrm{NF}(m = 1)$ with the carrier $\Psi_{②}(t)$, (c) $\mathrm{NF}(m = 1)$ with the carrier $\Psi_{③}(t)$ and (d) $\mathrm{NF}(m = 1)$ with the carrier $\Psi_{④}(t)$ $(\Delta\mathrm{T}/\mathrm{T_c} = 37\%)$. Theoretical calculations are based on the expressions of $G_{ps,m}$ and G_{pn} in Table I. Simulations are done based on a behavioral mixer model in ADS.

worthwhile to mention that in a single sideband carrier demodulation based on an ideal sinusoidal multiplication, NF will be 3 dB since noise is populating at double sidebands of a carrier while signal is residing at single sideband. The differential rectangular pulse of $\Psi_{③}(t)$ gives a near optimum NF of 3.36 dB with 37.1% of duty-cycle, as shown in Figs. 8(c) and 8(d).

IV. NOISE IN TIME-INTERLEAVED CARRIER DEMODULATION

A. Correlated and Uncorrelated Noises in Mixer Arrays

Consider two cases of TI-mixer arrays with a time-interleaving factor of M, shown in Fig. 9. In Fig. 9(a) each mixer will be driven by an individual current signal accompanied by a noise current which has no correlation among others, called '*uncorrelated-noise time-interleaved* (UNTI) mixer array'. The array can be transformed equivalently into a single mixer where an equivalent modulation carrier, $\Psi_{\mathrm{oc}}(t)$, can be synthesized by adding all delayed subcarriers of $\Psi_{\mathrm{ic}}(t)$. As discussed, the delay-sum operation of the subcarriers is inherently a filtering process with a transversal filter, which is illustrated in Fig. 10 for various types of subcarrier pulses. In Fig. 9(b) all the signal and noise currents are added before driving mixer array, and therefore each mixer will see the same unified single noise source which behaves like a correlated signal to the mixer array, called '*correlated-noise time-interleaved* (CNTI) mixer array'. The coherent signal currents are added linearly in current domain, increasing their magnitude by a factor or $\sqrt{M}$. But the uncorrelated noises will be added in power domain, effectively increasing their *rms* magnitude by a factor of in Fig. 9(b). In terms of the signal currents there is no difference between the two array topologies, and in the frequency domain the output signal will be

$$i_{os}(f) = i_s(f) \circledast \Psi_{ic} \circledast \mathrm{T}(f). \tag{17}$$

, where $\mathrm{T}(f)$ is the transfer function of the transversal filter given in (8). In view of noise, however, each mixer in the UNTI-mixer array will be driven by an *uncorrelated*

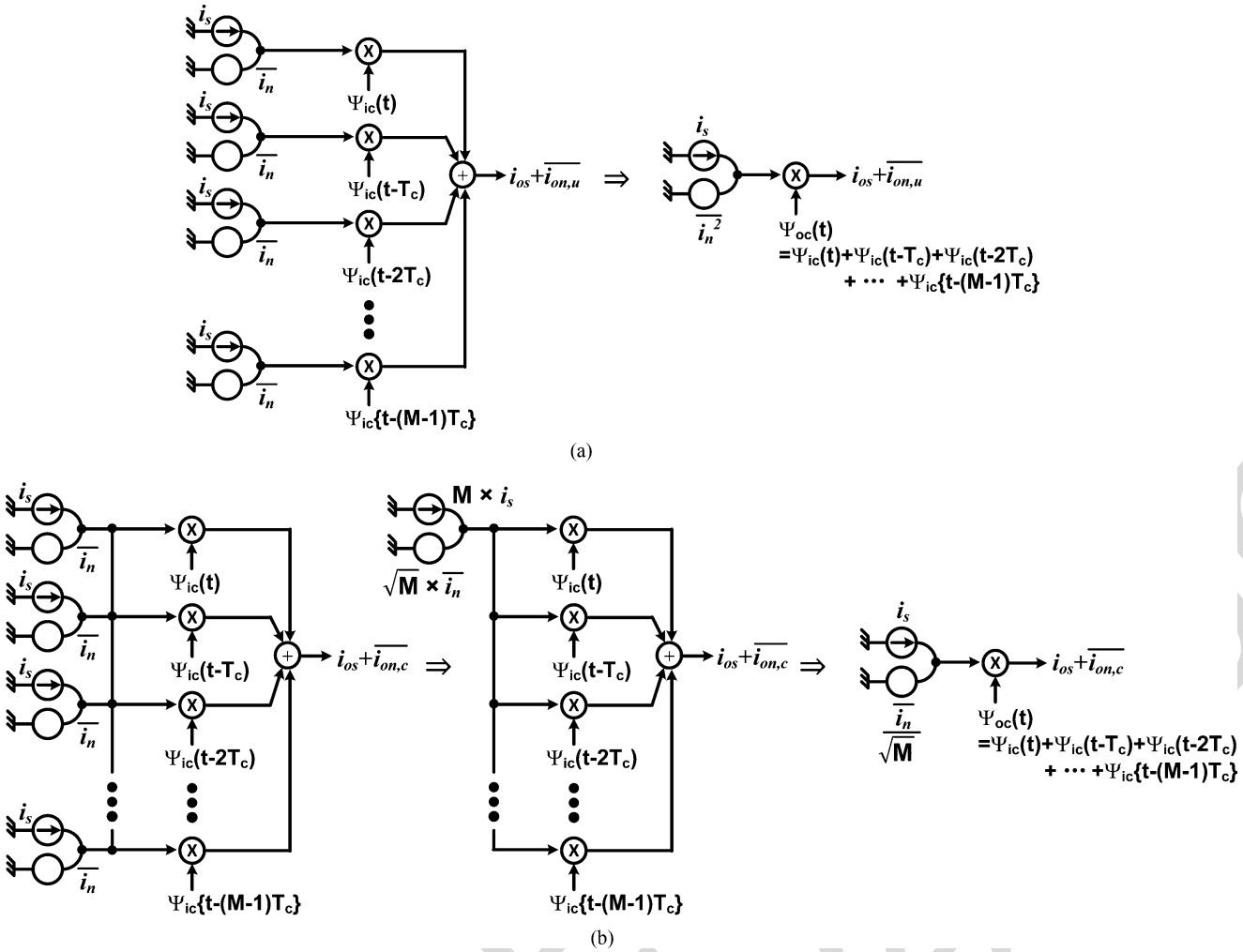

Fig. 9. Time-interleaved carrier modulation/demodulation with a time interleaving factor of M: (a) time-interleaved mixer array with uncorrelated noises to each mixer (UNTI-mixer array), (b) time-interleaved mixer array with correlated noises to each mixer (CNTI-mixer array).

noise and the net result is that all the subcarriers' fundamental and harmonic tones will involve in the noise demodulation. This effectively increases output noise power by a factor of the time-interleaving factor as expressed in (18). In the CNTI-mixer array in Fig. 9(b), each mixer is driven by a correlated noise. Therefore, only the subcarriers' spectral tones which are filtered in through the transversal filter will participate in the noise demodulation, which is expressed mathematically in (19).

$$\begin{aligned}
\overline{i_{on,u}(f)} &= \overline{i_n(f)} \circledast \Psi_{oc}(f) = \overline{i_n(f)} \circledast \Psi_{ic}(f)\,\mathrm{T}(f) \\
&\Rightarrow \overline{i_{on,u}{}^2(f)} = \overline{i_{on,u}(f)\, i_{on,u}(f)^*} \\
&= \overline{i_n{}^2} \circledast |\Psi_{ic}(f)|^2 \times M \\
&\Rightarrow G_{pn,u} = \frac{\overline{i_{on,u}{}^2(f)}}{\overline{i_n{}^2}} \\
&= M \times \sum_{m=-\infty}^{\infty} \left|\Psi_{ic}\left(\frac{m}{M} f_c\right)\right|^2 \qquad (18) \\
\overline{i_{on,c}(f)} &= \frac{\overline{i_n(f)}}{\sqrt{M}} \circledast \Psi_{oc}(f) = \frac{\overline{i_n(f)}}{\sqrt{M}} \circledast \Psi_{ic}(f) \circledast \mathrm{T}(f) \\
&\Rightarrow \overline{i_{on,c}{}^2(f)} = \overline{i_{on,c}(f)\, i_{on,c}(f)^*} \\
&= \frac{\overline{i_n{}^2}}{M} \circledast \left|\Psi_{ic}\left(\frac{m}{M} f_c\right) \frac{sin(m\pi)}{sin\left(\frac{m\pi}{M}\right)}\right|^2 \\
&\Rightarrow G_{pn,c} = \frac{\overline{i_{on,c}{}^2(f)}}{\overline{i_n{}^2}} \\
&= \sum_{m=-\infty}^{\infty} \frac{1}{M} \left|\Psi_{ic}\left(\frac{m}{M} f_c\right) \frac{sin(m\pi)}{sin\left(\frac{m\pi}{M}\right)}\right|^2 . \qquad (19)
\end{aligned}$$

In (18) and (19), $G_{pn,u}$ and $G_{pn,c}$ mean *uncorrelated* noise power gain and *correlated* noise power gain in each UNTI- and CNTI-mixer array, respectively. A net difference between the *correlated* and *uncorrelated* noises in TI-mixer arrays is that the *uncorrelated* noise will be added linearly versus the transversal filter length (or mixer array length) of M, while the *correlated* noise will be shaped by the transversal filter.

B. Duty-Cycle Control

In the TI-mixer arrays with M times of interleaving, the demodulation process relies on the M-th harmonic tone of the subcarrier spectrum. For each case of the subcarrier type illustrated in Fig. 10, Table II shows signal power gain and noise power gains for both cases of UNTI- and CNTI-mixer arrays.

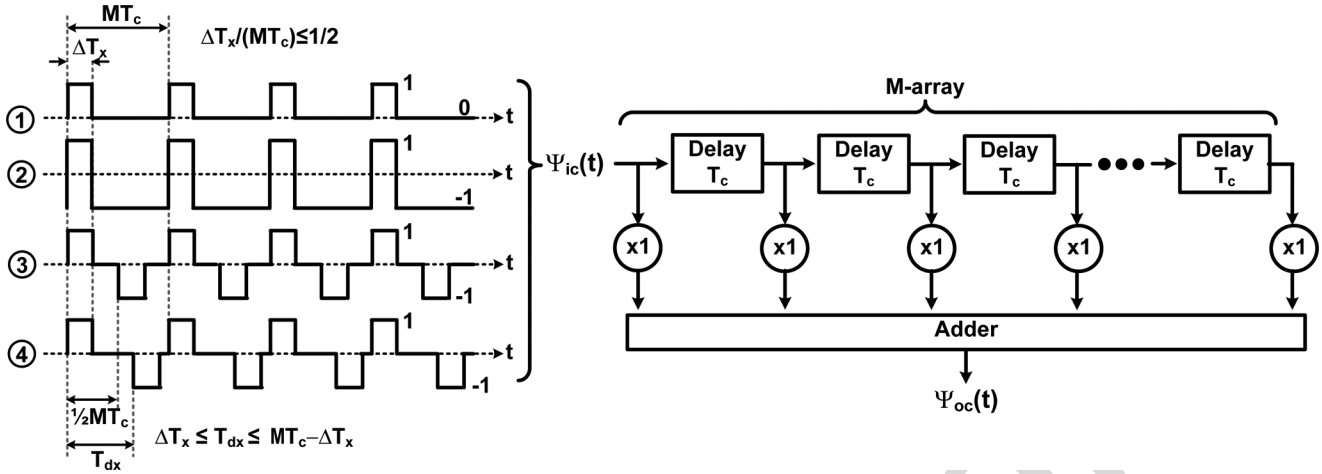

Fig. 10. Filtering rectangular carrier pulses using a transversal filter which is equivalent to the carrier synthesis based on the delay-sum operation in time-interleaved mixer arrays with M of time interleaving factor. ①: $\Psi_{s,①}(t)$- unipolar subcarrier pulse, ②: $\Psi_{s,②}(t)$- nonsymmetrical bipolar subcarrier pulse, ③: $\Psi_{s,③}(t)$—asymmetric bipolar differential ($\mathrm{T_dx} = 1/2\mathrm{MT_c}$ subcarrier pulse, and ④: $\Psi_{s,④}(t)$—asymmetric bipolar subcarrier pulse with an arbitrary T_{dx} under a constraint of $\Delta\mathrm{T_x} \leq \mathrm{T_{dx}} \leq \mathrm{MT_c} - \Delta\mathrm{T_x}$.

G_{ps},m is signal power gain when the demodulation is conducted by the m-th harmonic tone of the subcarriers. Because of a perfect correlation among the noises, noise power gain in the CNTI-mixer array (G_{pn},c in Table II) can be expressed in terms of the signal power gain, G_{pn},c, which can be much smaller than that G_{pn},u from the UNTI-mixer array. The term $(\sin m\pi/\sin m\pi/M)^2$ in $G_{ps,m}$ and $G_{pn,c}$ comes from the harmonic filtering function of the transversal filter inherited in the mixer array. The theoretical power gains in Table II have been verified through behavioral mixer array simulations in ADS, and typical results for $M = 3$ are shown in Fig. 11. $G_{ps,m}$ and $G_{pn,c}$ have a periodicity associated with the sinusoidal periodicity in $\sin(3\pi \times duty - cycle)$. Noise performance in the mixer arrays can be optimized by engineering duty-cycle of each subcarrier pulse. For UNTI-mixer arrays, with the same logics applied in (15), the optimum duty-cycle minimizing NF for each of the $\Psi_{s,①}(t)$, $\Psi_{s,②}(t)$ and $\Psi_{s,③}(t)$ in Fig. 10 can be found as

$$\left(\frac{\Delta T_x}{MT_c}\right)_{opt} \cong \frac{0.371}{\mathrm{m}}. \tag{20}$$

If a three-mixer array is used to utilize the 3rd-harmonic tone $(m = 3)$ of the subcarrier for demodulations, then the optimum duty-cycle will be $0.371/3 = 12.4\%$, which can be seen in the results shown in Figs. 11(a) and 11(c). As in fundamental mixers, a fully differential subcarrier (Fig. 11(c)) will exhibit the best SNR performance compared with the other types of subcarrier. For the differential subcarrier, 50% of duty-cycle is near optimum to get the maximum SNR. Note that in the time-interleaving technique with the differential subcarrier, signal power gain in the CNTI-mixer array can be larger than noise power gain. This process gain comes from the array configuration where by adding coherent signals and random noises before mixer arrays, effective SNR can be increased by the factor of the array length M, when compared with the SNR in a single mixer. From Fig. 11, it can also be confirmed that the SNR performance in the CNTI-array will be superior to that in the UNTI-array.

C. Noise Filtering

The optimization of duty-cycle to maximize SNR could be an economic solution for low frequency applications. However, it will be a challenging task to control the duty-cycle with a high accuracy at high frequencies, such as RF, microwave and millimeter-wave carrier modulations. As an alternative approach to the duty-cycle control, noise can be filtered out before the TI-demodulator arrays. A noise filter can be realized with an affordable manner at high frequencies using passive components.

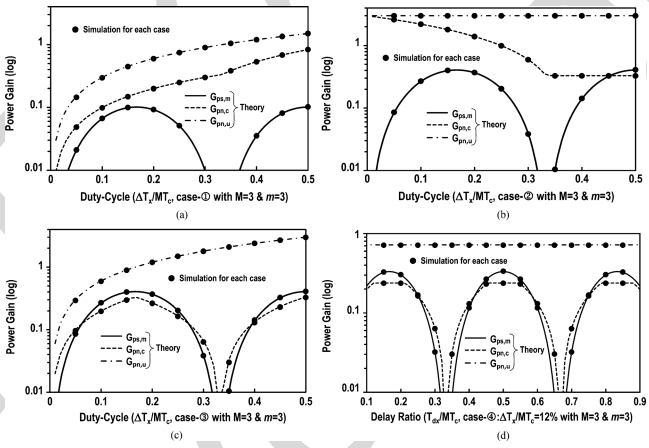

Fig. 11. Signal power gain, correlated noise power gain, and uncorrelated noise power gain for a 3-mixer array ($M = 3$) with various types of subcarriers described in Fig. 10(a) case with the unipolar subcarrier $\Psi_{s,①}(t)$ case with the nonsymmetrical bipolar subcarrier $\Psi_{s,②}(t)$, (c) case with the asymmetric differential bipolar subcarrier $\Psi_{s,③}(t)$, and (d) case with the asymmetric bipolar subcarrier $\Psi_{s,④}(t)$ with an arbitrary delay of $\mathrm{T_{dx}}$. Theoretical calculations are based on the expressions of $G_{ps,m}$ and $G_{pn,u}$ in Table II. Simulations are done based on a behavioral mixer model in ADS.

1) Bandpass Noise Filtering: Consider applying an ideal bandpass filtering to each TI-mixer array configuration in Fig. 9, which is illustrated in Fig. 12. To simplify discussion, let's assume that the bandpass filter (BPF) has a finite bandwidth (BW) extending over $f_s \pm 2f_{IF}$ centered at f_s. Suppose the demodulation is conducted by an ideal differential rectangular *subcarrier* of $\Psi_{s,③}(t)$ in Fig. 10 which has 50% duty-cycle with a fundamental frequency of $f_{c,sub} = (f_s + f_{IF})/M$. If the filter BW is smaller than $2 \times f_{c,sub}$, then the noise spectrum will not be aliased and the demodulation process will be equivalent to an ideal sinusoidal multiplication process. In such scenario, the M-th harmonic of $f_{c,sub}(= Mf_{c,sub} = f_s + f_{IF})$

TABLE II
SIGNAL POWER GAIN ($G_{\mathrm{ps,m}}$) AND NOISE POWER GAIN (G_{pn}) IN THE TIME-INTERLEAVED DEMODULATION PROCESS PERFORMED BY EACH CARRIER IN FIG. 10.

	$\mathbf{G_{ps,m}}$	$\mathbf{G_{pn,u}}$	$\mathbf{G_{pn,c}}$
①	$\left\{\frac{1}{m\pi}\sin\left(m\pi\frac{\Delta T_x}{MT_c}\right)\right\}^2\left(\frac{\sin m\pi}{\sin\frac{m\pi}{M}}\right)^2$	$\frac{\Delta T_x}{MT_c}\times M=\frac{\Delta T_x}{T_c}$	$\frac{1}{M}\sum_{m=-\infty}^{\infty}\left\{\frac{1}{m\pi}\sin\left(m\pi\frac{\Delta T_x}{MT_c}\right)\right\}^2\left(\frac{\sin m\pi}{\sin\frac{m\pi}{M}}\right)^2$
②	$\left\{\frac{2}{m\pi}\sin\left(m\pi\frac{\Delta T_x}{MT_c}\right)\right\}^2\left(\frac{\sin m\pi}{\sin\frac{m\pi}{M}}\right)^2$	M	$M\left(2\frac{\Delta T_x}{MT_c}-1\right)^2+\frac{2}{M}\sum_{m=1}^{\infty}\left\{\frac{2}{m\pi}\sin\left(m\pi\frac{\Delta T_x}{MT_c}\right)\right\}^2\left(\frac{\sin m\pi}{\sin\frac{m\pi}{M}}\right)^2$
③	$\left\{\frac{1}{m\pi}\sin\left(m\pi\frac{\Delta T_x}{MT_c}\right)\times(1-\cos m\pi)\right\}^2\left(\frac{\sin m\pi}{\sin\frac{m\pi}{M}}\right)^2$	$2\frac{\Delta T_x}{MT_c}\times M=2\frac{\Delta T_x}{T_c}$	$\frac{1}{M}\sum_{m=-\infty}^{\infty}\left\{\frac{1}{m\pi}\sin\left(m\pi\frac{\Delta T_x}{MT_c}\right)\times(1-\cos m\pi)\right\}^2\left(\frac{\sin m\pi}{\sin\frac{m\pi}{M}}\right)^2$
④	$\left\{\frac{\frac{1}{m\pi}\sin\left(m\pi\frac{\Delta T_x}{MT_c}\right)}{\times\sqrt{2-2\cos\left(2m\pi\frac{T_{dx}}{MT_c}\right)}}\right\}^2\left(\frac{\sin m\pi}{\sin\frac{m\pi}{M}}\right)^2$	$2\frac{\Delta T_x}{MT_c}\times M=2\frac{\Delta T_x}{T_c}$	$\frac{1}{M}\sum_{m=-\infty}^{\infty}\left\{\frac{\frac{1}{m\pi}\sin\left(m\pi\frac{\Delta T_x}{MT_c}\right)}{\times\sqrt{2-2\cos\left(2m\pi\frac{T_{dx}}{MT_c}\right)}}\right\}^2\left(\frac{\sin m\pi}{\sin\frac{m\pi}{M}}\right)^2$

***Note: ①, ②, ③, and ④ represent each subcarrier type depicted in Fig. 10, respectively.**

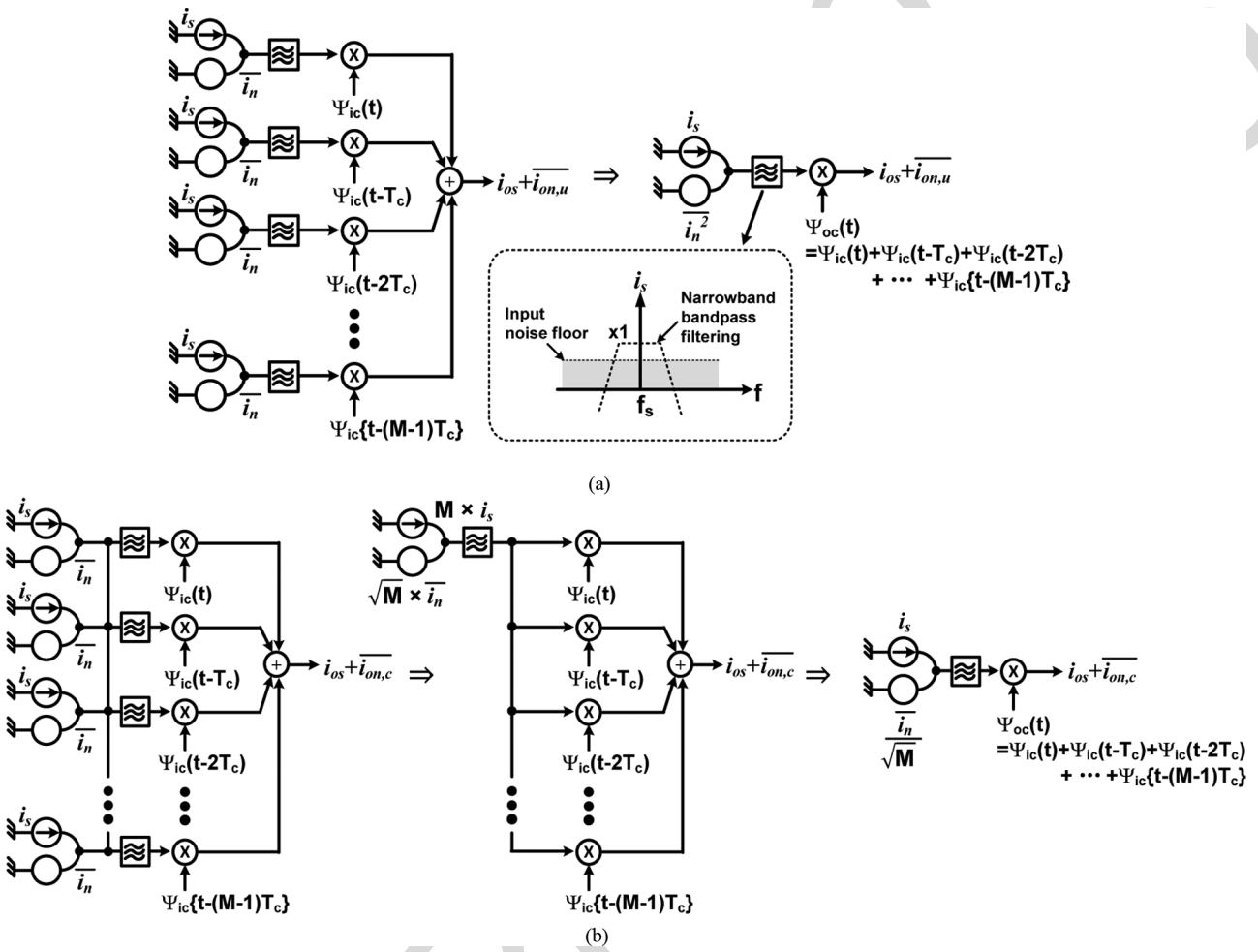

Fig. 12. Noise filtering in time-interleaved carrier modulations and demodulations: (a) time-interleaved demodulator array with filtering uncorrelated noises, (b) time-interleaved demodulator array with filtering correlated noises.

will demodulate the signal and noise. Output signal power gain will be $(2/\pi)^2$ for both cases UNTI- and CNTI-mixer arrays in Fig. 12. In view of noise the *uncorrelated* noise power gain in Fig. 12(a), given as $G_{pn,u}=\overline{i_{on,u}^2}/\overline{i_n^2}=(2/\pi)^2\times M$, will be the same as the *correlated* noise power gain in Fig. 12(b) given as $G_{pn,c}=\overline{i_{on,c}^2}/\overline{i_n^2}=(2M/\pi)^2\times 1/M$. When an ideal band-pass filtering is applied, the UNTI-mixer array will exhibit the same SNR as in the CNTI-mixer array. In real implementations, the BPF can be realized as a tuned load of RF front-end circuitry (e.g., LNAs) proceeding the mixer array.

2) Highpass Noise Filtering: While the BPF playing as an antialiasing noise filter guarantees an optimum output SNR in

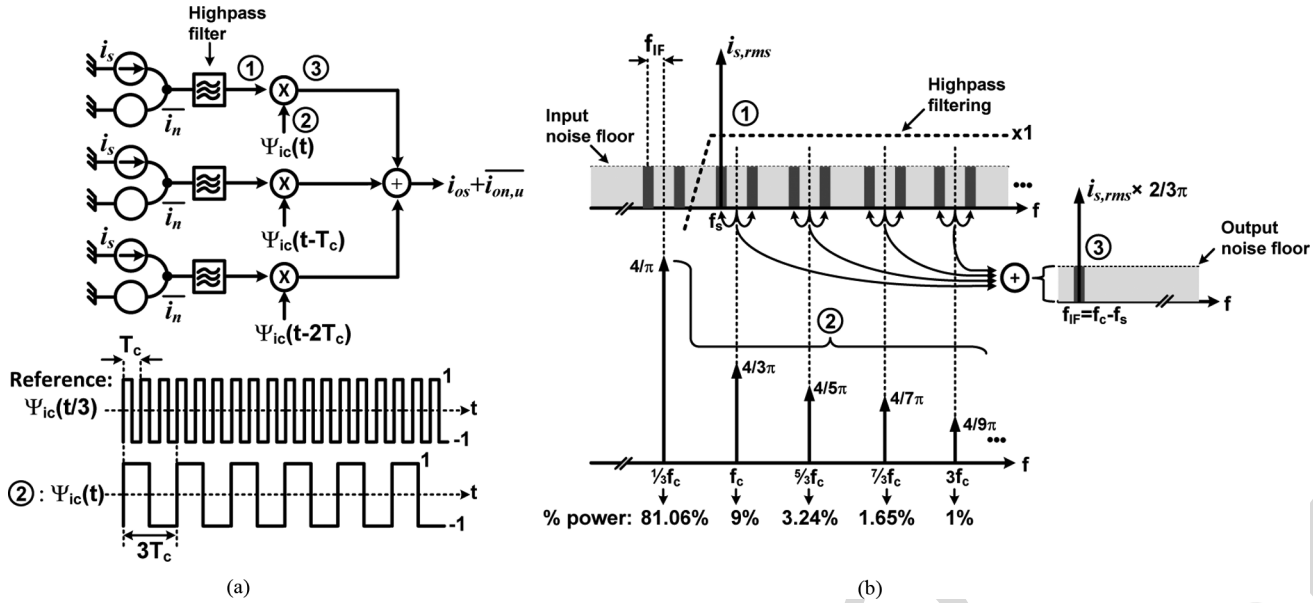

(a) (b)

Fig. 13. (a) Noise filtering around fundamental frequency of the *subcarrier* $\Psi_{\rm ic}(t)$ with a highpass filter in time-interleaved mixer array with a time interleaving factor $M = 3$, (b) conceptual description of spectral tones in the single path of the array.

TABLE III
SIGNAL POWER GAIN ($G_{\rm ps,m}$) AND NOISE POWER GAIN ($G_{\rm pn,u}$) AFTER HIGH-PASS NOISE FILTERING IN THE TIME-INTERLEAVED DEMODULATION PROCESS PERFORMED BY EACH CARRIER IN FIG. 10.

	$G_{pn,u}$	$G_{pn,c}$
①	$\left(\frac{\Delta T_x}{MT_c}-\left(\frac{\Delta T_x}{MT_c}\right)^2-2\sum_{k=1}^{M-1}\left\{(1-\delta_k{}^2)\left(\frac{1}{k\pi}\sin\left(k\pi\frac{\Delta T_x}{MT_c}\right)\right)^2\right\}\right)\times M$	$\frac{2}{M}\sum_{m=1}^{\infty}\left\{\frac{1}{m\pi}\sin\left(m\pi\frac{\Delta T_x}{MT_c}\right)\right\}^2\left(\frac{\sin m\pi}{\sin\frac{m\pi}{M}}\right)^2$
②	$\left(1-\left(1-\frac{2\Delta T_x}{MT_c}\right)^2-2\sum_{k=1}^{M-1}\left\{(1-\delta_k{}^2)\left(\frac{2}{k\pi}\sin\left(k\pi\frac{\Delta T_x}{MT_c}\right)\right)^2\right\}\right)\times M$	$\frac{2}{M}\sum_{m=1}^{\infty}\left\{\frac{2}{m\pi}\sin\left(m\pi\frac{\Delta T_x}{MT_c}\right)\right\}^2\left(\frac{\sin m\pi}{\sin\frac{m\pi}{M}}\right)^2$
③	$2\left(\frac{\Delta T_x}{MT_c}-\sum_{k=1}^{M-1}\left\{(1-\delta_k{}^2)\left(\frac{1}{k\pi}\sin\left(k\pi\frac{\Delta T_x}{MT_c}\right)\times(1-\cos k\pi)\right)^2\right\}\right)\times M$	$\frac{1}{M}\sum_{m=-\infty}^{\infty}\left\{\frac{1}{m\pi}\sin\left(m\pi\frac{\Delta T_x}{MT_c}\right)\times(1-\cos m\pi)\right\}^2\left(\frac{\sin m\pi}{\sin\frac{m\pi}{M}}\right)^2$
④	$2\left(\frac{\Delta T_x}{MT_c}-\sum_{k=1}^{M-1}\left\{(1-\delta_k{}^2)\left(\frac{\frac{1}{k\pi}\sin\left(k\pi\frac{\Delta T_x}{MT_c}\right)}{\times\sqrt{2-2\cos\left(2k\pi\frac{T_{dx}}{MT_c}\right)}}\right)^2\right\}\right)\times M$	$\frac{1}{M}\sum_{m=-\infty}^{\infty}\left\{\frac{\frac{1}{m\pi}\sin\left(m\pi\frac{\Delta T_x}{MT_c}\right)}{\times\sqrt{2-2\cos\left(2m\pi\frac{T_{dx}}{MT_c}\right)}}\right\}^2\left(\frac{\sin m\pi}{\sin\frac{m\pi}{M}}\right)^2$

***Note: ①, ②, ③, and ④ represent each subcarrier type depicted in Fig. 10, respectively.**

the TI-mixer array, highpass filter (HPF) can also improve the noise performance significantly in the UNTI-mixer arrays. This is illustrated conceptually in Fig. 13 for the case of $M = 3$ with an ideal differential rectangular subcarrier having 50% duty-cycle. Assuming a narrow IF-band in the array shown in Fig. 13(a), only the 3rd-harmonic tone (f_c) of the subcarrier $\Psi_{\rm ic}(t)$ demodulates signal to the IF-band and all the other tones involves noise aliasing. Noise modulation by the fundamental tone $(1/3f_c)$ of the subcarrier accounts for about 81% of total output noise power as illustrated in Fig. 13(b). Therefore, an ideal filtering out the noise around the fundamental tone by a HPF will improve the output SNR by 81%. The HPF will also reject DC noise in CNTI-array with unipolar subcarriers, reducing noise factor. However, for CNTI-array with bipolar differential subcarriers, the *correlated* noises around the fundamental tone will be filtered out already by the transversal filter inherited in the mixer array in ideal operation and extra filtering by the HPF will not improve the noise performance.

In general M-array with *uncorrelated* noises, noises residing lower sideband of the M-th harmonic tone of a subcarrier can be rejected by a HPF. Table III summarizes *correlated* and *uncorrelated* noise power gain after the highpass noise filtering when driven by different types of the subcarrier. In Table III, $(\Delta T_x/(MT_c))^2$ and $(1-2\Delta T_x/(MT_c))^2$ are the rejected DC powers by the HPFs when the array is driven by the subcarrier $\Psi_{\rm s,④}(t)$ and $\Psi_{\rm s,②}(t)$ in Fig. 10, respectively. In the table, δ_k ($k = 1$ to $M-1$) expresses finite rejection ratio of the k-th harmonic tone by the HPF: for example, $\delta_1 = 0.1$ means -20 dB of rejection for the fundamental tone $(= f_c/M)$ of the subcarrier.

The gain expressions in Table III have been verified with behavioral TI-mixer array simulations in ADS. Typical simulation results for $M = 3$ with the various types of subcarrier

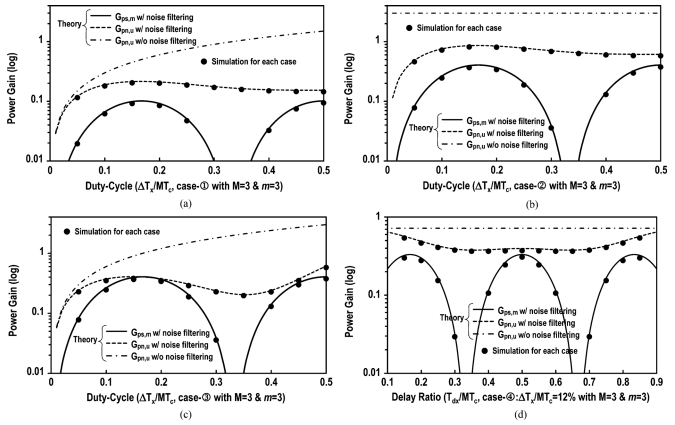

Fig. 14. Signal power gain and uncorrelated noise power gain after a highpass noise filtering for 3-mixer array ($M = 3$) with various types of subcarriers described in Fig. 10: (a) case with the unipolar subcarrier $\Psi_{\mathrm{s.}}(t)$, (b) case with the nonsymmetrical bipolar subcarrier $\Psi_{\mathrm{s.}}(t)$, (c) case with the asymmetric differential bipolar subcarrier $\Psi_{\mathrm{s.}}(t)$, and (d) case with the asymmetric bipolar subcarrier $\Psi_{\mathrm{s.}}(t)$ with an arbitrary delay of $\mathrm{T_{dx}}$. Theoretical calculations are based on the expressions of $G_{ps,m}$ and $G_{pn,u}$ in Table III. Simulations are done based on a behavioral mixer model in ADS.

depicted in Fig. 10 are shown in Fig. 14. The 3rd-order Butterworth-type HPF has been utilized in the behavioral simulations for the highpass noise filtering. In the simulation set-up, the signal frequency is $f_s = 120$ GHz, and the fundamental frequency of subcarrier is $f_c/M = 41$ GHz, resulting in $f_{IF} = 3$ GHz. The filter cut-off frequency is about 80 GHz, around the 2nd-harmonic tone of the subcarrier. Under the filter response, $\delta_1 = 0.134$ and $\delta_2 = 0.734$, which will reject about 98% and 46% of the fundamental noise power and the second-harmonic noise power, respectively, with a minimal loss for the signal. In Fig. 14, the theoretical $G_{pn,u}$ without noise filtering is also displayed together for a comparison purpose. There is a good agreement between the theory and behavioral simulation results. For every case, output noise power can be reduced by an order of magnitude with the noise filtering, while maintaining 50% of duty-cycle.

Finally, it is worthwhile to mention that the linearity performance, e.g., the 3rd order input intercept point ($\mathrm{IIP_3}$) or -1 dB gain compression point ($P_{-1\ \mathrm{dB}}$), of the mixer array would be better than a single mixer, assuming that the linearity performance of each individual mixer element in the array are the same as that of the single mixer. For instance, in the M-array the ($\mathrm{IIP_3}$) of the mixer array will be $10 \log M$ higher than the IIP3 of single mixer. This is because that in the M-element array, the effective input power for individual mixer will be M times smaller than the input power of the single mixer [22].

V. Error Analysis

A. Mismatch Analysis

Fig. 15 illustrates the array experiencing random gain mismatches and delay mismatches among the elements. $\Delta T_{\epsilon,\mathrm{n}}$ ($n = 1$ to $\mathrm{M}-1$) represents delay mismatch in each subcarrier from the reference subcarrier of $\Psi_{\mathrm{ic}}(t)$ shown as ①$\Delta w_{\epsilon,\mathrm{n}}$ ($n = 1$ to M-1) expresses gain mismatch in each array path with reference to the path gain which is modulated by the subcarrier ①. The random mismatches can be addressed as errors in the filter coefficients in the transversal filter. The gain mismatches are equivalently expressed as amplitude mismatches among the subcarriers. The $\Delta T_{\epsilon,n}$ and $\Delta w_{\epsilon,n}$ will originate from a device mismatch which is usually a random process having Gaussian statistics in electronics. Therefore, the $\Delta T_{\epsilon,n}$ and $\Delta w_{\epsilon,\mathrm{n}}$ can be treated as Gaussian random variables. Strictly speaking, they are independent among the array elements, requiring a joint probability of multiple random variables to describe the mismatch behavior in the TI-mixer array [23].

To simplify the discussion and to estimate the error in first order, following assumptions can be made. First, in real implementation a unit mixer will be repeated to form the mixer array, which means the $\Delta \mathrm{w}_{\epsilon,n}$ will have an equal 1σ-variance that can be expressed as $\overline{W_\varepsilon}$. In incorporating a successive delay in the subcarriers, an identical unit delay element can be cascaded and the variance of $\Delta T_{\epsilon,n}$ will be same in each delay element, which can be represented as $\overline{\tau_\varepsilon}$. The worst case scenario will be that the $\Delta w_{\epsilon,n}$ and $\Delta T_{\epsilon,n}$ have a perfect correlation among the mixer elements and the delay cells. In the worst case scenario, the variance of $\Delta T_{\epsilon,n}$ will be accumulated linearly when propagating the delay chain in Fig. 15. These assumptions are reflected in the transversal filter transfer function, $\mathrm{T}_\varepsilon(f)$ in (21) at the bottom of the following page, where the mismatch random variables are incorporated in the complex weights in the first step and then each random variable is approximated to its 1σ-variance. Note, $\overline{W_\varepsilon}$ and $\overline{\tau_\varepsilon}$ can be treated as another Gaussian random variables which are common to each mixer and delay element. $\overline{W_\varepsilon}$ and $\overline{\tau_\varepsilon}$ will have the same statistical properties as $\Delta w_{\epsilon,n}$ and $\Delta T_{\epsilon,\mathrm{n}}$, respectively.

Usually the random mismatches are weak perturbations and it will be a reasonable assumption that $1 \gg \overline{\tau_\varepsilon}/T_c$. This allows $e^{-jm\pi(1+\overline{\tau_\varepsilon}/T_c)} \cong e^{-jm\pi} = cosm\pi$ in (21), resulting in the approximation of the magnitude response of the transversal filter transfer function as

$$|\mathrm{T}_\varepsilon(f)| = |\mathrm{T}_\varepsilon\left(\frac{m}{MT_c}\right)|, m = integer$$
$$\cong 1 + \left(1+\overline{W_\varepsilon}\right)\cos m\pi \left(\frac{\sin\left(\frac{m\pi}{M}\left(1+\frac{\overline{\tau_\varepsilon}}{T_c}\right)(M-1)\right)}{\sin\left(\frac{m\pi}{M}(1+\frac{\overline{\tau_\varepsilon}}{T_c})\right)}\right). \tag{22}$$

The output signal, $i_{os,\varepsilon}(f)$, under the finite mismatches in the array will be

$$i_{os,\varepsilon}(f) = i_s(f)\,\Psi_{ic}(f)\,\mathrm{T}_\varepsilon(f). \tag{23}$$

The signal power gain $G_{ps,m}$ under the mismatches can be found by replacing $(\sin m\pi/\sin m\pi/M)^2$ with $|\mathrm{T}_\varepsilon(f)|^2$ in Table II and Table III. The *uncorrelated* noise power gain under the mismatches in UNTI-mixer arrays, $G_{pn,u\varepsilon}$ corresponding to $G_{pn,u}$ in (18), can be given as

$$\overline{i_{on,u\varepsilon}(f)} = \overline{i_n(f)}\Psi_{ic}(f)\,\mathrm{T}_\varepsilon(f)$$
$$\overline{{i_{on,u\varepsilon}}^2(f)} = \overline{i_{on,u\varepsilon}(f)\,i_{on,u\varepsilon}(f)^*}$$
$$= \overline{{i_n}^2}|\Psi_{ic}(f)|^2\left\{1+\sum_{\beta=1}^{M-1}\left(1+\overline{W_\varepsilon}\right)^2\right\}$$

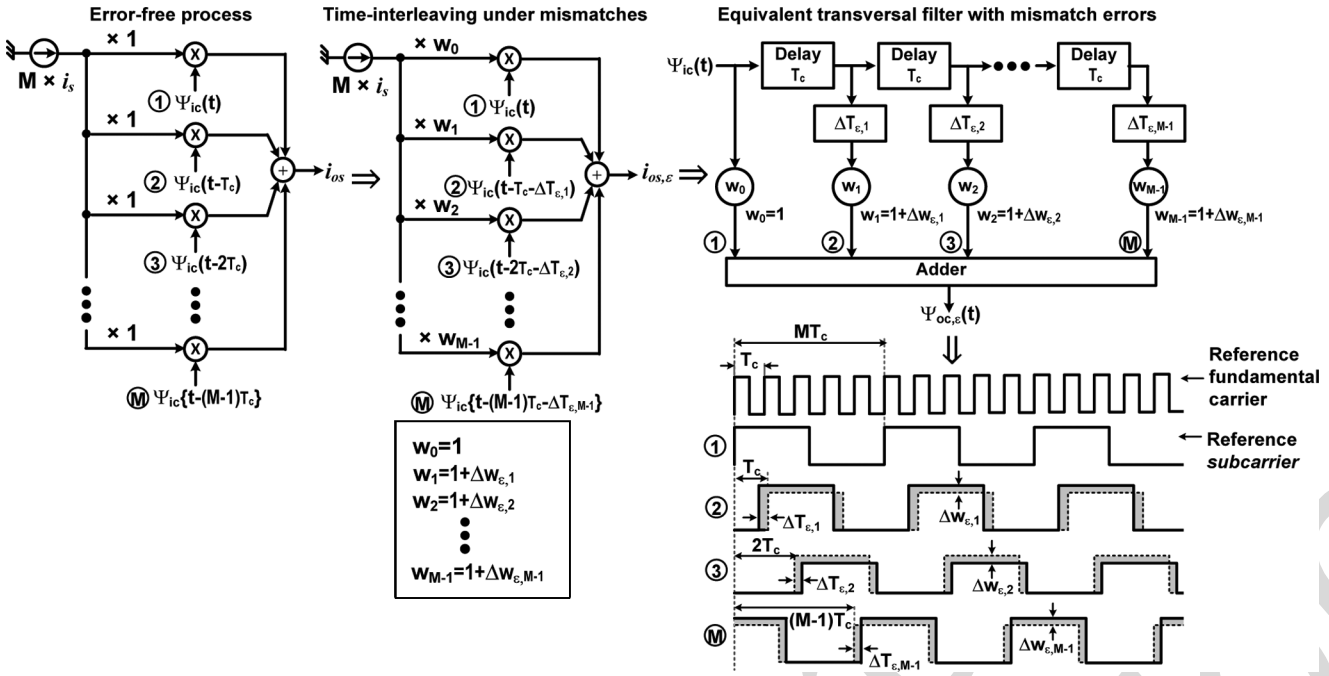

Fig. 15. Time-interleaving process with errors from gain and delay mismatches among the array elements (the dotted rectangular pulses are ideal subcarriers). $\Delta T_{\varepsilon,n}$ ($n = 1$ to M-1) represents delay mismatch in each subcarrier with reference to the subcarrier of ①. $\Delta w_{\varepsilon,n}$ ($n = 1$ to M-1) expresses gain mismatch from in each array path with reference to the path modulated by the subcarrier of ①.

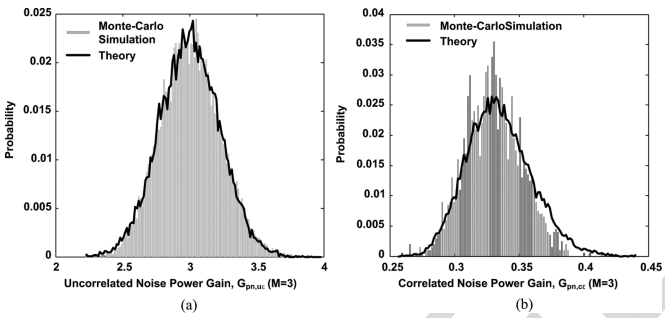

Fig. 16. Statistical mismatch simulation results of noise power gains in the TI-mixer arrays without noise filtering ($M = 3$, duty-cycle of subcarriers $= 50\%$): (a) UNTI-mixer array, and (b) CNTI-mixer array. Bar graphs are the results from Monte-Carlo simulations in ADS. 1σ-variance of $\overline{\tau_\varepsilon} = \pm 2\%$ and 1σ-variance of T_c of (equivalently $\pm 2.4^\circ$ of 1σ phase-variance).

$$G_{pn,u\varepsilon} = \left\{1 + \left(1 + \overline{W_\varepsilon}\right)^2 (M-1)\right\} \sum_{m=-\infty}^{\infty} |\Psi_{ic}(f)|^2$$
$$\cong \left\{M + 2(M-1)\overline{W_\varepsilon}\right\} \sum_{m=-\infty}^{\infty} |\Psi_{ic}\left(\frac{m}{MT_c}\right)|^2. \quad (24)$$

It should be noted that due to a lack of coherence among the noises in the UNTI-mixer arrays, the output noise power and therefore $G_{pn,u\varepsilon}$ is not dependent of phase mismatches, but proportional to the variance of the amplitude mismatches. For the CNTI-mixer arrays in Fig. 9(b), the *correlated* noise power gain under the mismatches, $G_{pn,c\varepsilon}$ corresponding to in (19), will be approximated as (25), shown at the bottom of the page.

$$\mathrm{T}_\varepsilon(f) = \mathrm{T}_\varepsilon\left(\frac{m}{MT_c}\right), m = integer$$
$$= 1 + \sum_{\beta=1}^{M-1} \underbrace{\left((1 + \Delta w_{\varepsilon,\beta})\, e^{-j2m\pi\Delta T_{\varepsilon,\beta}/MT_c}\right)}_{\substack{\Delta \\ complex\ weight}} e^{-j2m\beta\pi/M}$$
$$\cong 1 + \sum_{\beta=1}^{M-1} \underbrace{\left(\left(1 + \overline{W_\varepsilon}\right) e^{-j2m\beta\pi\overline{\tau_\varepsilon}/MT_c}\right)}_{\substack{\Delta \\ \Delta w_{\varepsilon,\beta} \cong \overline{W_\varepsilon} \\ \Delta T_{\varepsilon,\beta} \cong \beta\overline{\tau_\varepsilon}}} e^{-j2m\beta\pi/M}$$
$$= 1 + \left(1 + \overline{W_\varepsilon}\right)\left(\frac{sin\left(\frac{m\pi}{M}\left(1 + \frac{\overline{\tau_\varepsilon}}{T_c}\right)(M-1)\right)}{sin\left(\frac{m\pi}{M}\left(1 + \frac{\overline{\tau_\varepsilon}}{T_c}\right)\right)}\right) e^{-jm\pi(1+\overline{\tau_\varepsilon}/T_c)} \quad (21)$$

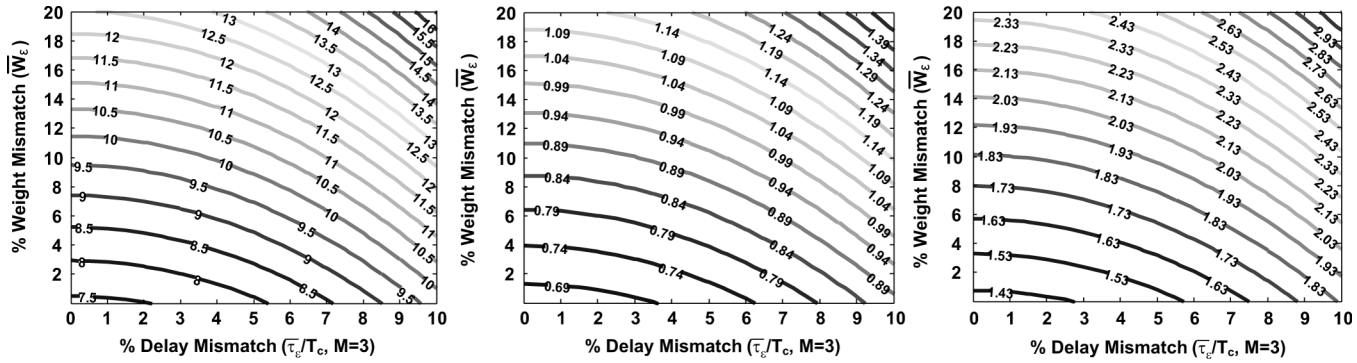

Fig. 17. Contour plots of the noise factor, $F(m=3)$ in (13), of UNTI-mixer arrays with $M=3$ (duty-cycle: 50%) under weight and delay mismatches: (a) noise factor without noise filtering, (b) noise factor with an ideal bandpass noise filtering, and (c) noise factor with an ideal high-pass noise filtering (only fundamental tone, , is rejected by an ideal HPF).

B. Mismatch Behavioral Simulations

The mismatch models have been verified through Monte-Carlo (MC) mismatch simulations in ADS. Typical simulation results are shown in Fig. 16 for the case of $M=3$. The differential subcarrier $\Psi_{s,\textcircled{1}}(t)$ with 50% duty-cycle is utilized. It can be confirmed from the MC simulations that the worst case error distribution happens when $\Delta w_{\varepsilon,1}$ and $\Delta w_{\varepsilon,2}$ have a perfect correlation; and $\Delta T_{\varepsilon,\beta}$ ($\beta=1$ and 2) in Fig. 15 accumulates coherently across the delay chain as discussed. For a conservative estimation, the Gaussian mismatch variables have been set as following in the ADS MC simulations: two independent variables of $\Delta w_{\varepsilon,1}$ and $\Delta w_{\varepsilon,2}$ are set as the same variable with $\pm 5\%$ of 1σ–variance; and $\Delta T_{\varepsilon,2} = 2\Delta T_{\varepsilon,1}$ where $\Delta T_{\varepsilon,1}/T_c$ has $\pm 2\%$ of 1σ–variance and $\Delta T_{\varepsilon,2}/T_c$ has $\pm 4\%$ of 1σ–variance, respectively. Figs. 16(a) and 16(b) show probability distributions after 2000 ADS MC runs for each case of UNTI- and CNTI-mixer arrays, respectively. The theoretical distributions in Fig. 16 have been estimated using (24) and (25) in MATLAB statistical simulations: 1σ–variances of $\overline{W_\varepsilon}$ and $\overline{\tau_\varepsilon}/T_c$ are 5% and 2%, respectively. There is a good agreement between the ADS MC simulations and the theoretical estimations.

For the UNTI-array $(M=3)$ under the weight and delay mismatches, noise factor $F(m=3)$ has been calculated based on (23) and (24). Fig. 17 displays contour plots of the noise factors which are well agreed with ADS behavioral simulation results. Fig. 17(a) show the noise factor without noise filtering. Figs. 17(b) and 17(c) are the cases with an ideal bandpass and highpass noise filtering, respectively. As expected, the TI-mixer array with *uncorrelated* noises exhibits a high sensitivity to the mismatches (reference: when and without noise filtering, F(3)= $3/0.405 = 7.4$). The bandpass and highpass noise filtering, however, reduce the sensitivity to the mismatches dramatically in the UNTI-mixer array. From ADS MC simulations, it can also be confirmed that in CNTI-mixer arrays sensitivity to mismatches can be reduced substantially by a bandpass noise filtering as well.

VI. Conclusions

This paper proposes a time-interleaved carrier modulation and demodulating technique. The present method is essentially a mixer array technique relying on a parallel interleaving of a series of modulated outputs in the time domain. The time-interleaved mixer array inherits a filtering function from a transversal filter, and the time interleaving process is equivalent to a selective filtering of a fundamental tone and its harmonics of carrier signals. A carrier waveform and duty-cycle play a critical role in the noise performance of the arrays, and a comprehensive noise analysis is presented for both correlated and uncorrelated noises. Analytical mismatch models are provided and verified through ADS Monte-Carlo simulations. The time-interleaved array technique will allow a high-speed in carrier modulations and demodulations with a trade off a system complexity. It will be a promising solution to realize high-frequency frequency mixing systems extending over millimeter and sub-millimeter wave regime under a limitation of active device speed.

$$\begin{aligned}
\overline{i_{on,c\varepsilon}(f)} &= \frac{\overline{i_n(f)}}{\sqrt{M}} \circledast \Psi_{ic}(f) \circledast \mathrm{T}_\varepsilon(f) \\
&= \frac{\overline{i_n^2}}{M} |\Psi_{ic}(f)\,\mathrm{T}_\varepsilon(f)|^2 \\
G_{pn,c\varepsilon} &\cong \sum_{m=-\infty}^{\infty} \left(\begin{array}{c} \frac{1}{M} \times \left|\Psi_{ic}\left(\frac{m}{MT_c}\right)\right|^2 \times \\ \left(1+\left(1+\overline{W_\varepsilon}\right)\cos m\pi \left(\frac{\sin\left(\frac{m\pi}{M}\left(1+\frac{\overline{\tau_\varepsilon}}{T_c}\right)(M-1)\right)}{\sin\left(\frac{m\pi}{M}\left(1+\frac{\overline{\tau_\varepsilon}}{T_c}\right)\right)}\right)\right)^2 \end{array} \right)
\end{aligned} \tag{25}$$

REFERENCES

[1] "IEEE standard 802.15.3c, wireless medium access control (MAC) and physical layer (PHY) specifications for high rate wireless personal area network (WPANs)," *Amendment 2: Millimeter-Wave Based Alternative Physical Layer Extension, Ratified 12*, Oct. 2009.

[2] A. Hirata, T. Kosugi, H. Takahashi, J. Takeuchi, H. Togo, M. Yaita, N. Kukutsu, K. Aihara, K. Murata, Y. Sato, T. Nagatsuma, and Y. Kado, "120-GHz-Band wireless link technologies for outdoor 10-Gbit/s data transmission," *IEEE Trans. Microw. Theory Tech.*, vol. 60, no. 3, pp. 881–895, Mar. 2012.

[3] J. Federici and L. Moeller, "Review of terahertz and subterahertz wireless communications," *J. Appl. Phys.*, vol. 107, no. 11, p. 111101, Jun. 2010.

[4] S. K. Reynolds, "A 60-GHz superheterodyne downconversion mixer in silicon-germanium bipolar technology," *IEEE J. Solid-State Circuits*, vol. 39, no. 11, pp. 2065–2068, Nov. 2004.

[5] A. Parsa and B. Razavi, "A new transceiver architecture for the 60-GHz band," *IEEE J. Solid-State Circuits*, vol. 44, no. 3, pp. 751–762, Mar. 2009.

[6] F. Vecchi, S. Bozzola, M. Pozzoni, D. Guermandi, E. Temporiti, M. Repossi, U. Decanis, and A. Mazzanti, "A wideband mm-Wave CMOS receiver for Gb/s communications employing interstage coupled resonators," *Proc. ISSCC Dig. Tech. Papers*, pp. 220–221, Feb. 2010.

[7] B. R. Jackson and C. E. Saavedra, "A CMOS ku-band 4x subharmonic mixer," *IEEE J. Solid-State Circuits*, vol. 43, no. 6, pp. 1351–1359, Jun. 2008.

[8] H. Takahashi, T. Kosugi, A. Hirata, K. Murata, and N. Kukutsu, "10-Gbit/s quadrature phase-shift-keying modulator and demodulator for 120-GHz-Band wireless links," *IEEE Trans. Microw. Theory Tech.*, vol. 58, no. 12, pp. 4072–4078, Dec. 2010.

[9] J.-D. Park, S. Kang, and A. M. Niknejad, "A 0.38 THZ fully integrated transceiver utilizing a quadrature push-push harmonic circuitry in sige bicmos," *IEEE J. Solid-State Circuits*, vol. 47, no. 10, pp. 2344–2354, Oct. 2012.

[10] K. W. Kobayashi, A. K. Oki, L. T. Tran, J. C. Cowles, G. Gutierrez-Aitken, F. Yamada, T. R. Block, and D. C. Streit, "A 108-GHz InP-HBT monolithic push-push VCO with low phase noise and wide tuning bandwidth," *IEEE J. Solid-State Circuits*, vol. 34, no. 9, pp. 1225–1232, Sep. 1999.

[11] K. K. O, M. C. F. Chang, M. Shur, and W. Knap, "Sub-millimeter wave signal generation and detection in CMOS," in *Proc. MTT-S Int. Microw. Symp. Dig.,–188*, Jun. 2009, p. 185.

[12] E. Seok, D. Shim, C. Mao, R. Han, S. Sankaran, C. Cao, W. Knap, and K. K. O, "Progress and challenges towards terahertz CMOS integrated circuits," *IEEE J. Solid-State Circuits*, vol. 45, no. 8, pp. 1554–1563, Aug. 2010.

[13] W. C. Black and D. A. Hodges, "Time interleaved converter arrays," *IEEE J. Solid-State Circuits*, vol. SC-15, no. 12, pp. 1022–1029, Dec. 1980.

[14] C. S. G. Conroy, D. W. Cline, and P. R. Gray, "An 8-b 85-MS/s parallel pipeline A/D converter in 1-mm CMOS," *IEEE J. Solid-State Circuits*, vol. 28, 4, no. 4, pp. 447–454, Apr. 1993.

[15] D. Camarero, K. B. Kalaia, J.-F. Naviner, and P. Loumeau, "Mixed-signal clock-skew calibration technique for time-interleaved adcs," *IEEE Trans. Circuits Syst. I, Reg. Papers*, vol. 55, no. 11, pp. 3676–3687, Dec. 2008.

[16] A. V. Oppenheim, R. W. w. Schafer, and J. R. Buck, *Discrete-Time Signal Processing*, 2nd ed ed. Upper Saddle River, NJ, USA: Prentice Hall, 1999.

[17] *Advanced Design System (ADS)*. Santa Clara, CA, USA: Agilent Technology Inc..

[18] L. W. Couch, *Digital and Analog Communication Systems*, 6 ed. Upper Saddle River, NJ, USA: Prentice Hall, 2000.

[19] K.-J. Koh, M.-Y. Park, C.-S. Kim, and H.-K. Yu, "Subharmonically pumped CMOS frequency conversion (up and down) circuits for 2-GHz WCDMA direct-conversion transceiver," *IEEE J. Solid-State Circuits*, vol. 39, no. 6, pp. 871–884, Jun. 2004.

[20] H.-C. Chen, T. Wang, H.-W. Chiu, Y.-C. Yang, T.-H. Kao, G.-W. Huang, and S.-S. Lu, "A 5-GHz-band CMOS receiver with low LO self-mixing front end," *IEEE Trans. Circuits Syst. I, Reg. Papers*, vol. 56, no. 4, pp. 705–713, Apr. 2009.

[21] S. He and C. E. Saavedra, "An Ultra-Low-Voltage and Low-Power $\times 2$ Subharmonic Downconverter Mixer," *IEEE Trans. Microw. Theory Tech.*, vol. 60, no. 2, pp. 311–317, Feb. 2012.

[22] R. V. Gatti, M. Dionigi, and R. Sorrentino, "Computation of gain, noise figure, and third-order intercept of active array antenna," *IEEE Trans. Antennas Propagat.*, vol. 52, no. 11, pp. 3139–3142, Nov. 2004.

[23] P. Z. Peebles, *Probability, Random Variables, and Random Signal Principles*, 3 ed. New York, NY, USA: McGraw-Hill, 1993.

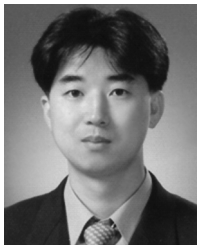

Kwang-Jin Koh (S'06–M'09) received the B.S. degree in electronic engineering (first-class honors) from Chung-Ang University, Seoul, Korea, in 1999, the M.S. degree in electrical engineering from the Korea Advanced Institute of Science and Technology (KAIST), Daejeon, Korea, in 2001, and the Ph.D. degree in electrical and computer engineering from the University of California at San Diego, La Jolla, CA, USA, in 2008.

In November 2011, he joined the Electrical and Computer Engineering Department, Virginia Polytechnic Institute and State University (Virginia Tech), Blacksburg, as an Assistant Professor. From 2001 to 2004, he was with the Electronics and Telecommunications Research Institute (ETRI), Daejeon, Korea, where he was engaged in the research and development of RF and analog CMOS integrated circuits for wireless communication systems. From 2008 to 2010, he was with the Portland Technology Group (PTD), Intel Corporation, as a Senior Engineer, where he was involved in the development of voltage-controlled oscillators (VCOs) and phase-locked loops (PLLs) in Intel 32- and 22-nm CMOS processes for Intel microprocessors and radios applications. From 2010 to 2011, he was with the Broadcom Corporation, as a Senior Staff Scientist, where he developed RF integrated circuits (RFICs) for digital TV tuner systems-on-a-chip. His research interests include analog, RF and millimeter-wave integrated circuits and systems wireless communications, radars, and imaging applications.

Dr. Koh was the recipient of the 2002 Best Paper Award of the IEEE Solid-State Circuits Society and Electron Device Society, Seoul Chapter. His Ph.D. works on integrated phased arrays on silicon technologies have been reported to the U.S. Pentagon as part of a Defense Advanced Research Projects Agency (DARPA) War Report as one of the major accomplishments of 2007. He was also the recipient of the 2010 Best Team of the Year Award of the Teledyne Scientific Corporation (formerly the Rockwell Scientific Corporation), and 2012 Virginia Tech ICTAS Junior Faculty Research Award.

Seyed Yahya Mortazavi (S'07) received the B.S. degree in electrical engineering from University of Tehran, Tehran, Iran, in 2003 and the M.S. degree in electrical engineering from Tarbiat-Modares University, Tehran, Iran, in 2005. The M.S. research was on high-speed folding-Interpolating ADC design, and continued on wide-bandwidth high-resolution sigma-delta ADCs until 2010. He is currently working toward the Ph.D. degree in electrical engineering at Virginia Tech (VT), Blacksburg, VA, USA.

His research interests include system and circuit design for RF and mm-Wave integrated communication transceivers, and Imaging systems.

Sadia Afroz (S'10) received the B.S. degree in electrical engineering from Bangladesh University of Engineering and Technology, Bangladesh, in 2011. She is currently working toward the Ph.D. degree at Virginia Tech, Blacksburg, VA, USA.

Her research was on high-speed Ultra wideband Inter and intra-chip wireless communication system until 2011. Her current research interests include design of millimeter-wave circuits, wireless transceiver and Phased-array architectures.